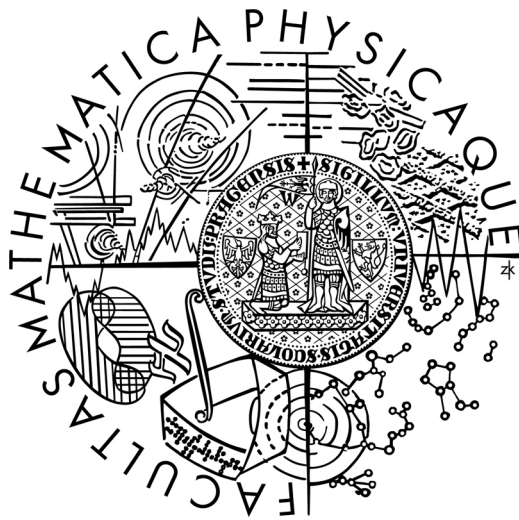Charles University in Prague
Faculty of Mathematics and Physics

DIPLOMA THESIS

Adela Grohol'ová

Luminescence spectroscopy of two-dimensional quantum structures in the GaAs/AlGaAs system

Institute of Physics of Charles University

Supervisor: *Assoc. Prof. Roman Grill, PhD.*

Study program:
Optics and optoelectronics

Acknowledgement

I confess that I have written my diploma thesis on my own and using only the quoted sources. I agree with lending the diploma thesis.

Prague, August 9, 2006

Adela Grohoľová

Contents

Název práce: ***Luminiscenční spektroskopie dvojdimenzionálních kvantových struktur v systému GaAs/AlGaAs***
Autor: ***Adela Grohoľová***
Katedra (ústav): ***Fyzikální ústav Univerzity Karlovy***
Vedoucí diplomové práce: ***Doc. RNDr. Roman Grill, CSc.***
E-mail vedoucího: ***grill@karlov.mff.cuni.cz***

Abstrakt: Cílem této práce je studium fotoluminiscenčních vlastností dvojité kvantové jámy v systému GaAs/Al$_{0.33}$Ga$_{0.67}$As. Jsou proměřena nízkoteplotní luminiscenční spektra v závislosti na elektrickém a magnetickém poli a rozdílné excitační intenzitě. K tomu jsou proměřeny i teplotní závislosti luminiscence zejména nepřímých excitonů v podélném magnetickém poli. Aby se vysvětlil rozpor ohledně útlumu fotoluminiscence nepřímých excitonů v podélném magnetickém poli, je diskutován jednoduchý model lokalizovaných nepřímých excitonů. Z pozorovaného Zeemanova štěpení jsou spočteny hodnoty efektivních g-faktorů pro nepřímý, neutrální a nabitý exciton. K vysvětlení jejich chování je navrženo několik jednoduchých modelů. Je diskutována případná shoda či rozpor s jinými doposud publikovanými experimentálními daty.
Klíčová slova: Dvojitá kvantová jáma, GaAs/AlGaAs, Fotoluminiscence, Exciton, Landého g-faktor

Title: ***Luminescence spectroscopy of two-dimensional quantum structures in the GaAs/AlGaAs system***
Author: ***Adela Grohoľová***
Department: ***Institute of Physics of Charles University***
Supervisor: ***Assoc. Prof. Roman Grill, PhD.***
Supervisor's e-mail address: ***grill@karlov.mff.cuni.cz***

Abstract: The aim of this work is the study of photoluminescence properties of GaAs/Al$_{0.33}$Ga$_{0.67}$As double quantum well. Low-temperature luminescence spectra of this sample are measured in dependence on electric and magnetic field and different excitation power. The temperature dependencies of photoluminescence especially of the indirect excitons in in-plane magnetic field are gauged as well. The simple model of localized indirect excitons is discussed to explain the discrepancy concerning the damping of indirect exciton photoluminescence in in-plane magnetic field. The effective g-factors of indirect, neutral and charged excitons are calculated from observed Zeeman splitting. Few simple models are proposed to explain the behavior of effective g-factors. The possible agreement or contradiction with other published experimental data is discussed.
Keywords: Double quantum well, GaAs/AlGaAs, Photoluminescence, Exciton, Landé g-factor

Chapter 1

Introduction

Two-dimensional quantum systems encourage attention of academic and industrial world since their first fabrication in 1973. They manage many interesting and unique physical properties (high mobility of electrons, integral and fractional quantum Hall effect, phenomena connected with electron-nuclear spin coupling, etc.). Therefore they have been a subject of intensive study and research. Many techniques, such as photoluminescence, photoluminescence excitation and photoconductivity, are used to achieve some useful results. Two-dimensional quantum systems promise a big use in many technical applications. Some of them were already realized (semiconductor lasers, transistors, etc.). Apart from many research workplaces all over the world Institute of Physics of Charles University in co-operation with Institute of Physics of the ASCR and Institute of Technical Physics I of Friedrich-Alexander University in Erlangen, Germany, participates in a fundamental research of these interesting quantum systems.

Under words "two-dimensional quantum structures" one can understand either a wide class of quantum wells or superlattices. The main purpose of this diploma thesis was to study double quantum wells by photoluminescence spectroscopy using the external electric and magnetic fields. We studied one sample consisting of a symmetric double quantum well. In this paper we present our measurement in in-plane magnetic field up to 9.6 T completed with temperature and excitation intensity dependencies as well as our polarization-distinguished measurements of effective Landé g-factor of neutral and charged excitons.

Chapter 2

Two-dimensional quantum structures

As mentioned in previous chapter our measurements were done on a system of symmetric double quantum well. Therefore we would like to summarize some basic properties of a single well and double quantum wells in this chapter. Under the word quantum well we will understand an one-dimensional potential well used to trap particles. This arbitrary system must be characterized by two-dimensional translation symmetry. From now on we will respect this notation: z is the direction of growth, normal to the planes of a layered structure, and its direction is always marked as perpendicular. Direction parallel to the plane layers of a structure is always called longitudinal.

2.1   The idealized single quantum well

In this section we will discuss the solution of Schrödinger equation for one-dimensional square quantum well. Our survey will be very similar to the lecture from quantum mechanics, for details see [1]. Using the term idealized we mean that the carrier mass m in such structures is both position and energy independent. We use V_0 and d to denote the depth and the width of the quantum well, respectively. $\mathcal{H}$ denotes the Hamiltonian of the system. The corresponding Schrödinger equation is

$$i\hbar\frac{\delta\psi(z,t)}{\delta t} = \mathcal{H}(z,p_z)\psi(z,t), \tag{2.1}$$

where

$$\mathcal{H}(z,p_z) = \frac{p_z^2}{2m} + V(z), \qquad p_z = -i\hbar\frac{\delta}{\delta z}. \tag{2.2}$$

Symbol $\hbar$ marks as usually the reduced Planck constant ($\hbar = 1.05457 \times 10^{-34}$ J s). We take the origin in the middle of the well so that $V(z) = 0$ in the region $|z| \geq d/2$ and $V(z) = -V_0$ in the region $|z| < d/2$. Since Hamiltonian does not explicitly depend on time we can factorize the wavefunction $\psi(z,t)$ into

$$\psi(z,t) = \chi(z)\exp(-\frac{i}{\hbar}\varepsilon t). \tag{2.3}$$

Function $\chi(z)$ must satisfy the eigenvalue problem (it solves the time-independent Schrödinger equation)

$$\mathcal{H}(z, p_z)\chi(z) = \varepsilon\chi(z), \tag{2.4}$$

which can be written more explicitly

$$\left[-\frac{\hbar^2}{2m}\frac{d^2}{dz^2} + V(z)\right]\chi(z) = \varepsilon\chi(z). \tag{2.5}$$

Since potential $V(z)$ is even (our choice of the origin) we can look for either even or odd functions $\chi(z)$. Inside the well we can write:

$$\chi(z) = A\cos k_w z; \qquad \varepsilon = -V_0 + \frac{\hbar^2 k_w^2}{2m} \qquad \text{for even states} \tag{2.6}$$

$$\chi(z) = B\sin k_w z; \qquad \varepsilon = -V_0 + \frac{\hbar^2 k_w^2}{2m} \qquad \text{for odd states.} \tag{2.7}$$

k_w denotes the wavevector of the particle inside the well. The region outside the well is prohibited for particles therefore the wavefunction $\chi(z)$ must damp down in the barrier. This is expressed by decreasing exponentials. Simultaneously the wavefunction $\chi(z)$ must fulfil following boundary conditions:

- $\chi(z)$ and $\frac{d\chi(z)}{dz}$ is continuous everywhere;

- $\lim\limits_{z \to \pm\infty} |\chi(z)| = 0$.

Applying these boundary conditions at $z = \frac{d}{2}$ we find out that the energy ε satisfies the transcendental equations

$$k_w \tan\left(k_w \frac{d}{2}\right) = \kappa_b \qquad \text{for even states} \tag{2.8}$$

$$k_w \cot\left(k_w \frac{d}{2}\right) = \kappa_b \qquad \text{for odd states.} \tag{2.9}$$

κ_b stands for the wavevector associated with the evanescent waves outside the well

$$\kappa_b = \sqrt{-\frac{2m\varepsilon}{\hbar^2}}. \tag{2.10}$$

The discrete quantum mechanical spectrum of the energy ε is in contrast with the classical continuous spectrum. A quantum well of thickness d admits $n(d)$ bound states where:

$$n(d) = 1 + \text{Int}\left[\sqrt{\frac{2mV_0 d^2}{\pi^2\hbar^2}}\right], \tag{2.11}$$

Int$[x]$ denotes the integer part of x. As can be seen from Eq. (2.11) a one-dimensional quantum well always supports at least one bound state, irrespective of the height of the confining barrier. In Fig. 2.1 we can see the first bound state of the single quantum well of the height V_0 and width d. It is the first even state.
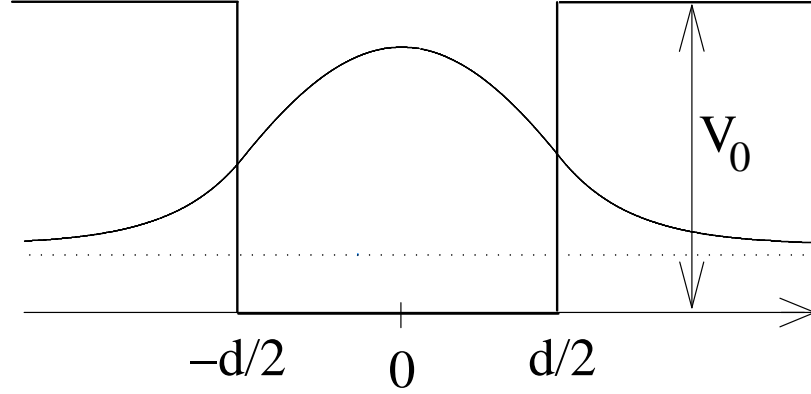
Figure 2.1: The ground state of the single quantum well of the height V_0 and width d.

2.1.1 Density of states

The density of states $\rho(\varepsilon)$ is a physical quantity which gives a number of quantum states $|\nu\rangle$ per unit energy and unit area available around a given energy ε.

$$\rho(\varepsilon) = \frac{1}{S} \sum_\nu \delta(\varepsilon - \varepsilon_\nu), \tag{2.12}$$

where ε_ν is the energy associated with the state $|\nu\rangle$. Based on the parabolic bands assumption the formula for $\rho(\varepsilon)$ results in the two-dimensional quantum structures as:

$$\rho(\varepsilon) = \frac{m}{\pi\hbar^2} \sum_n Y(\varepsilon - E_n); \qquad E_n < 0, \tag{2.13}$$

where $Y(x)$ is the step function defined $Y(x)=1$ if $x > 0$ and $Y(x)=0$ if $x < 0$, S is the sample area. Because of the step function $Y(x)$ the density of states $\rho(\varepsilon)$ is staircase-shaped.

2.2 The symmetric double quantum well

After the small summary of the basic properties of the idealized single quantum well we will briefly outline the topic of the symmetric double quantum well (DQW). This will consist of two equivalent one-dimensional quantum wells of depth V_0 and width d which are separated by a distance h. The corresponding Hamiltonian of the coupled wells reads

$$\mathcal{H} = \frac{p_z^2}{2m} + V(z - z_1) + V(z - z_2), \tag{2.14}$$

where

$$V(z - z_i) = \begin{cases} 0 & |z - z_i| \geq d/2, \\ -V_0 & |z - z_i| \leq d/2. \end{cases} \tag{2.15}$$

$i = 1, 2$ and z_i corresponds to the centre of respective wells.

2.2.1   The tight binding approximation

When h is high enough we get two isolated wells with the ground state eigenfunctions $\chi_1(z - z_1)$ and $\chi_1(z - z_2)$ for the wells centered at $z = z_1$ and $z = z_2$, respectively. As the exact solution of Eq. (2.14) we can take the linear combination of the eigenfunctions $\chi_\nu(z - z_i)$ of the individual wells where ν runs over the discrete and continuous spectra. To obtain a simple formula for energy ε of the double quantum well system we retain only a linear combination of the ground states of the isolated wells:

$$\psi(z) = \alpha\chi_1(z - z_1) + \beta\chi_1(z - z_2). \tag{2.16}$$

This technique is known as the tight binding approximation. We let now the Hamiltonian (2.14) to act on the function (2.16). Using the matrix representation we obtain:

$$\begin{bmatrix} E_1 + s - \varepsilon & (E_1 - \varepsilon)r + t \\ (E_1 - \varepsilon)r + t & E_1 + s - \varepsilon \end{bmatrix} \begin{bmatrix} \alpha \\ \beta \end{bmatrix} = 0, \tag{2.17}$$

where E_1 is the energy of the ground state of the isolated well. The quantities r, s and t are called the overlap (r), shift (s) and transfer (t) integrals, respectively and they are defined as follows:

$$r = \langle\chi_1(z - z_1)|\chi_1(z - z_2)\rangle = \langle\chi_1(z - z_2)|\chi_1(z - z_1)\rangle \tag{2.18}$$

$$s = \langle\chi_1(z - z_1)|V(z - z_2)|\chi_1(z - z_1)\rangle = \langle\chi_1(z - z_2)|V(z - z_1)|\chi_1(z - z_2)\rangle \tag{2.19}$$

$$t = \langle\chi_1(z - z_1)|V(z - z_1)|\chi_1(z - z_2)\rangle = \langle\chi_1(z - z_2)|V(z - z_2)|\chi_1(z - z_1)\rangle. \tag{2.20}$$

Using some simple mathematical manipulations we obtain from Eq. (2.17) the formula for energy ε of the double quantum well in the scope of the tight binding approximation:

$$\varepsilon = E_1 \mp \frac{t}{1 \mp r} + \frac{s}{1 \mp r}. \tag{2.21}$$

From the Eq. (2.21) we can see that the energy of the ground state of the isolated well E_1 is shifted to a new value $E_1 + \frac{t}{1+r}$ due to the presence of the other well.

2.2.2   The exact solution of the symmetric DQW

As can be found in [1] to obtain the exact eigenstates of the symmetric double quantum well we need to solve the following equation:

$$2\cos k_w d + \left(\xi - \frac{1}{\xi}\right)\sin k_w d \pm \left(\xi + \frac{1}{\xi}\right)\exp(-\kappa_b h)\sin k_w d = 0, \tag{2.22}$$

where

$$\xi = \frac{\kappa_b}{k_w}; \qquad \kappa_b = \sqrt{\frac{-2m\varepsilon}{\hbar^2}}; \qquad k_w = \sqrt{\frac{2m}{\hbar^2}(\varepsilon + V_0)}. \tag{2.23}$$

The sign plus in Eq. (2.22) corresponds to the antisymmetric states, the sign minus corresponds to the symmetric states (with respect to the center of the structure). Similarly to the single quantum well the double quantum well also supports always at least one bound state.

2.3 Quantum wells in real heterostructures

This section will pay attention to the real heterostructures, semiconductors composed of more than one material. Also alloys can be used to obtain the desired physical properties. Nowadays many heterostructures are extensively used in optoelectronical applications. To be able to decide which materials are the best to create almost an idealized heterostructure one need to consider the band structure and the lattice constant of both materials. Especially in optoelectronics some particular wavelengths are required and the band gap parameter is of great importance.

So called *Vegard's law* is usually used to calculate a lattice constant of the $Al_xGa_{1-x}As$ alloy:

$$a_{Al_xGa_{1-x}As} = xa_{AlAs} + (1 - x)a_{GaAs}. \tag{2.24}$$

In our heterostructures we use a pair of the most popular materials, GaAs and AlGaAs. Their lattice constants are very similar, their change is less than 0.15% as function of x. Thus it is possible to let them grow on each other almost without stress on their interfaces. This is valid for any intermediate alloy of $Al_xGa_{1-x}As$.

2.3.1 Growth of real heterostructures

There are two dominant ways in today's industry for making heterostructures. The first one is called molecular beam epitaxy (MBE) and the second one is metal-organic chemical vapour deposition (MOCVD). Both are in principle simple techniques but there are too many parameters which must be controlled. So far our samples were prepared by MBE in Erlangen, Germany, we describe shortly the MBE technique only.

The scheme of MBE apparatus is displayed in Fig. 2.2. It consists of an evaporator, a heated holder for the substrate, several Knudsen cells containing material for deposition with shutters on the top and RHEED (reflected high-energy electron diffraction) accessory for monitoring the growth of the heterostructure. There is an ultrahigh vacuum (UHV) in the whole apparatus assuring that molecules of vaporized elements (e.g. Ga, Al and As) would not collide with each other and that they would produce a molecular beam. This beam is pointed to the heated holder on the substrate that can rotate during the growth. This way we can minimize possible variations in composition across the wafer. The beams are controlled through the shutters. Once they are opened the growth can start or proceed. The flux of vaporized elements is controlled through the temperature of the cell.

Now RHEED description follows. An electron gun is used to proceed high-energy electrons that are directed at nearly grazing incidence to the surface of the sample. The intensity and pattern of diffracted electrons are displayed on a screen. They change in a periodic way as step by step each monolayer is grown. Thus we can count monolayers precisely and from the diffraction pattern we can deduce the structure of the surface.
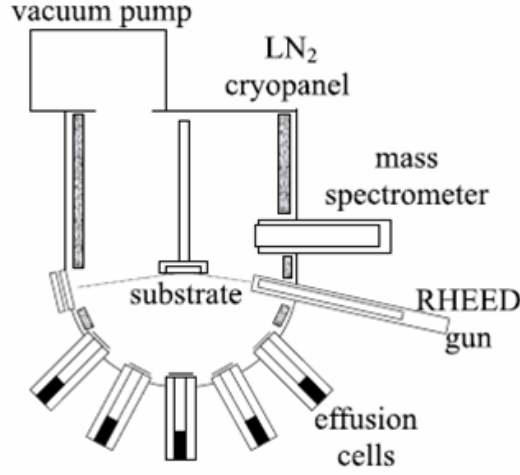
Figure 2.2: The scheme of molecular beam epitaxy apparatus.

The speed of MBE is approximately 1 monolayer per second. To obtain a high-quality sample one should start with pure materials in Knudsen cells. Every possible pollution devastates the physical properties of the final heterostructure.

2.3.2 Layered structures

The compounding of different materials during MBE growth is advantageously used at a preparation of heterostructures with a particular band gap structure. The band gap of an $Al_xGa_{1-x}As$ alloy can be counted via the formula:

$$E_g^{Al_xGa_{1-x}As}\,(\text{meV}) = E_g^{GaAs}\,(\text{meV}) + 1240x\,(\text{meV}); \qquad x < 0.45. \qquad (2.25)$$

Nowadays three alignments according to the band gap structure are known, type I or straddling alignment, type II or staggered alignment and finally type III or broken-gap alignment. To get a basic idea about these notions please see Fig. 2.3.

Our sample GaAs/AlGaAs shows type I alignment which is usually described by *Anderson's rule*. This rule states that the vacuum levels of the two materials should be lined up, as we can see in Fig. 2.4. From this figure we see that offset ΔE_C of the conduction band is equal to the difference between the electron affinity χ of the two materials (an electron affinity is the energy an electron from the conduction band minimum needs to get to the vacuum level). The offset ΔE_V is then given by the equation:

$$\Delta E_V = \Delta E_g - \Delta E_C. \qquad (2.26)$$

In our sample with the Al barrier content $x = 0.33$ the band offsets $\Delta E_C \doteq 230$ meV and $\Delta E_V \doteq 150$ meV are commonly used.
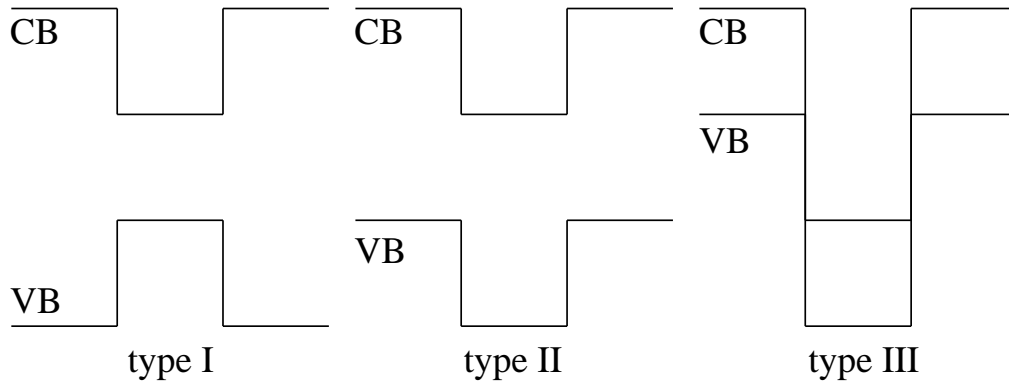
Figure 2.3: Three types of possible alignment according to the band gap structure. CB denotes the conduction band, VB stands for valence band.
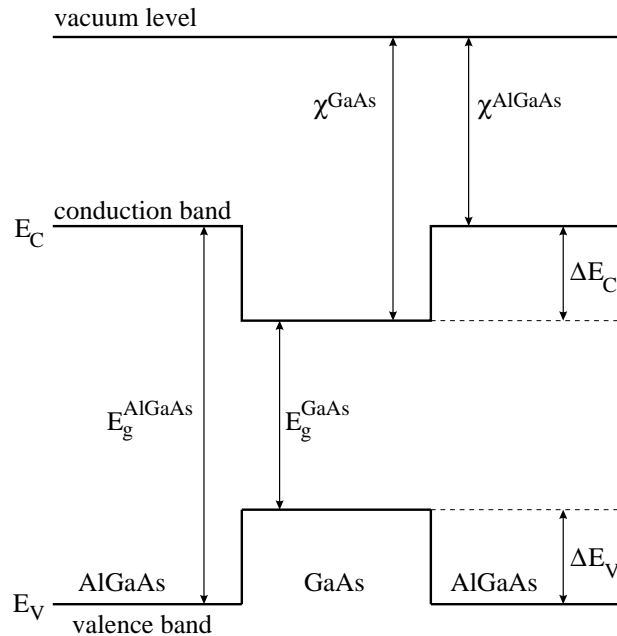
Figure 2.4: The scheme of quantum well in the system GaAs/AlGaAs which is a typical example of alignment type I.

With the help of MBE the simple profiles can be grown. The most famous are the tunneling barrier and the quantum well. Specifically for our materials, a tunneling barrier consists of a layer of AlGaAs surrounded by GaAs. A quantum well is the opposite of the barrier and consists of a thin layer of GaAs surrounded by two thick layers of AlGaAs.

2.3.3 Modulation doping

In some optoelectronical devices there is a need to have many free particles, for example free electrons, apart from their dopants. To solve this requirement so called modulation doping is often used. Its principle is based on the transfer of carriers from the remote wide-gap doped region to the narrow-gap undoped one.

In case there is a discontinuity in conduction bands the travelling electrons/holes lose their potential energy after entering the region of the narrow gap material. They become trapped in this area as it is not possible for them to climb over the barrier ΔE_C. Consequently, free carriers are separated from their doping counterparts. The electrostatic potential of charged dopants attracts carriers back to the doped region. However, due to the discontinuity in the conduction bands the electrons can not return to their donors. They are only pressed to the interface where they are trapped in the triangular potential well. As we could see from the previous section the energy levels are quantized in a quantum well. Thus the electrons can occupy the same state for motion in z direction but they remain free in other two dimensions. The two-dimensional electron gas (2DEG) is formed in this way. The modulation doping has provided us with two positive outcomes:

- the electrons are separated from their donors $\Rightarrow$ scattering by ionized impurities is reduced,

- the electrons are confined to two dimensions.

The separation between electrons and donors can be supported by putting a spacer layer between the doped and undoped region.

Chapter 3

Quantum structures subject to the electric field

The research of the effects of the applied external electric field on the quantum structures gives us the opportunity to construct the optoelectronical devices such as fast electro-optical modulators, etc. The effects induced by electric field are very often called the *Stark effect.* In quasi two-dimensional structures two kinds of Stark effect are possible. The electric field can be applied either parallel to the growth axis z or perpendicular to it. As in our experiments the electric field was always applied parallel to the growth axis z we discuss only this type of Stark effect in this thesis.

3.1   The transverse electric field

The corresponding Hamiltonian of the system with applied electric field F along z axis can be written as follows:

$$\mathcal{H} = \frac{p_x^2}{2m} + \frac{p_y^2}{2m} + \frac{p_z^2}{2m} + V(z) - qFz. \tag{3.1}$$

We use m to denote the mass of the particle and assume that it is the same in the well and in the barrier. q denotes the charge of the particle. For an electron $q = -|e|$, for a hole $q = |e|$, ($e = -1.602 \times 10^{-19}$ C is the charge of the electron). As we can see from Eq. (3.1) in plane (x, y) the motion of the particle is not restricted so we will concentrate only on the solution of the one-dimensional problem:

$$\left[-\frac{\hbar^2}{2m} \frac{d^2}{dz^2} - qFz \right] \chi(z) = E\chi(z). \tag{3.2}$$

The general form of the solution of Eq. (3.2) is the combination of the Airy functions which are continuously extended in the points of the potential jump. Nevertheless, this form is a little bit complicated. One can simplify it with assumption of the
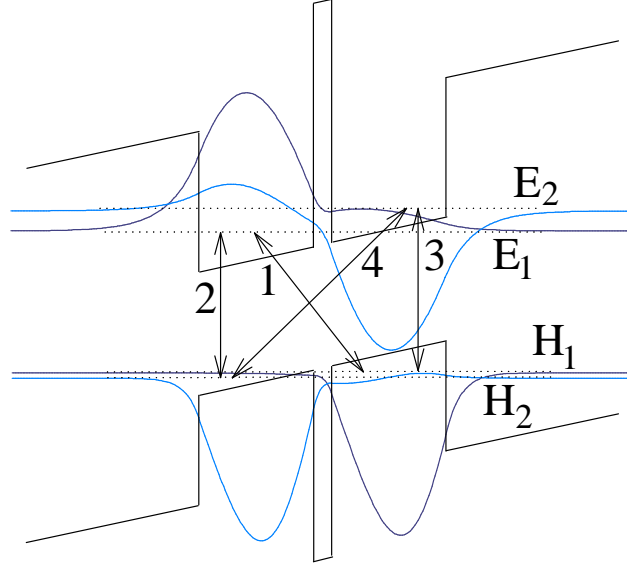
Figure 3.1:   The basic diagram of the interband recombination in the DQW under an external electric field action. Symbols $E_{1,2}$, $H_{1,2}$ mark the two lowest lying energy levels of electrons and holes, respectively. Numbers 2 and 3 (1 and 4) denote the spatially direct (indirect) electron-hole recombination, respectively. After reference [3].

damping exponentials everywhere outside the well. Applying the external electric field on the quantum well the well gets to the tilted position as we can see in Fig. 3.1. The particle inside the well becomes essentially localized by a triangular well. In case the barrier height is finite with increasing electric field the particle accumulation is never complete. The field-induced tunneling appears (when F is sufficiently large) and the particle is swept out from the quantum well.

The absorbed light from a diode laser generates pairs of free particles. The carriers are excited in the GaAs as well as in the $Al_x Ga_{1-x} As$ layers. Applying the bias voltage the excited carriers are transported into the wells and to the surface of the sample. Consequently, bound complexes such as neutral excitons, positively or negatively charged excitons can be formed in the whole volume of the sample.

As the charge of the electrons and holes is of the opposite sign the electrons become localized in the opposite part of the well than the holes. The electrons always prefer to occupy the states with lower energy, mostly they are localized on the energy level E_1. Similarly, the holes always prefer to occupy the states with higher energy, mostly they are localized on the energy level H_1. For details see Fig. 3.1.

Due to the Coulomb interaction the exciton can be formed from an electron and a hole. Let us assume that an electron with energy E_1 from the left well and a hole with energy H_2 as well from the left well are bound together into an exciton. In this case we call it spatially direct exciton and use DX to denote it. Numbers 2 and 3 mark the spatially direct electron-hole recombination in Fig. 3.1. The energy of DX

transition E_1 - H_2 is almost independent on the applied bias. Thus the DX peak should always appear approximately at the same energy in our spectra. We see DX transitions in our PL spectra in zero magnetic field in Fig. 7.1.

The spatially indirect exciton is formed when an electron from one well is bound to a hole from the adjacent well. Symbol IX stands for the indirect excitons. In Fig. 3.1 numbers 1 and 4 denote the indirect transitions. The energy levels E_1 and H_1 are approaching each other (the energy of the indirect transitions decreases) when the bias voltage increases. Thus the energy of IX peak is always lower than the energy of DX peak and depends strongly on applied bias voltage. Our measured spectra show this behavior, see Fig. 7.1.

3.2 The transverse electric field in the tight binding approximation

To obtain some simple formulas for energy levels in the symmetric DQW we can again use the tight binding approximation as we did in Subsection 2.2.1. At the beginning we make some assumptions and set some symbols to clear our notation. We take $k_{\parallel} = 0$ for simplicity. Symbols z_R (z_L) denote the center of the right (left) well with respect to the origin of coordinates, respectively. We express the influence of the electric field with the shift of the energy levels of the isolated quantum wells:

$$E_{R,L}^{\nu}(F) = E_{R,L}^{\nu}(F = 0) - qF z_{R,L}. \tag{3.3}$$

Furthermore we assume that other energy levels are far away from the ground states. Therefore we take the same linear combination of the ground states (2.16) of the isolated wells as we did in Subsection 2.2.1. In addition to that we assume that shift integral s and overlap integral r, defined in 2.2.1, are equal to zero. With all these simplifications we can write the formula for eigenenergies of symmetric DQW:

$$E_{1,2} = E_1 \pm \sqrt{\frac{(qF\Delta)^2}{4} + t^2}, \tag{3.4}$$

where E_1 is the energy of the ground state of the isolated well, t is transfer integral defined in 2.2.1 and $\Delta = z_R - z_L$. Index 1 (2) belongs to the sign "+" ("−"), respectively.

The eigenfunctions of the symmetric DQW in the presence of electric field are given by the linear combination $|\Psi\rangle = a(F)|\chi_1(z - z_1)\rangle + b(F)|\chi_1(z - z_2)\rangle$. Applied electric field brakes the original symmetry of the Hamiltonian of DQW. So originally symmetric DQW behaves as asymmetric in the presence of electric field.

Chapter 4

Quantum structures subject to the magnetic field

Magnetic field can be applied on the two-dimensional (2D) quantum structure in two main directions: parallel (so called *Voigt orientation*) or perpendicular (*Faraday orientation*) to the plane layers. In this chapter we will give a brief overview of the basic relevant theory. To introduce magnetic field into the corresponding Hamiltonian we replace the operator of the particle momentum $\vec{p}$ in the Schrödinger equation with the operator $(\vec{p} - \frac{q}{c}\vec{A})$ as the operators of the kinetic and canonical momentum are not the same in the external electromagnetic field. Here we omit the interaction between the spin of an electron and magnetic field $\vec{B}$ as next chapter is set aside to inform about Zeeman splitting.

4.1 Perpendicular magnetic field

In this section we will have a look at the 2D quantum systems subjected to the perpendicular magnetic field $\vec{B} = (0, 0, B)$. There are many possibilities how to choose the vector potential $\vec{A}$ which corresponds to a given field B. However all results should be gauge-invariant and depend only on B. We choose so called *Landau gauge* of the vector potential $\vec{A} = (0, Bx, 0)$ in which there is the simplest algebra. Applying the magnetic field $\vec{B}$ the Hamiltonian of 2D system changes into

$$\mathcal{H} = \frac{p_x^2}{2m} + \frac{(qBx)^2}{2m} + \frac{p_y^2}{2m} - \frac{qBp_yx}{m} + \frac{p_z^2}{2m} + V(z). \tag{4.1}$$

From the Eq. (4.1) we can see that the Hamiltonian is y-independent. This fact allows us to write the wavefunction $\Psi(\vec{r})$ in the following form:

$$\psi(\vec{r}) = \frac{1}{\sqrt{S}} \exp(ik_y y)\varphi(x)\chi(z), \tag{4.2}$$

13

where S is the sample area. The Schrödinger equation becomes

$$\left[\frac{p_x^2}{2m} + \frac{1}{2}m\omega_C^2(x - x_0)^2 + \frac{p_z^2}{2m} + V(z)\right]\varphi(x)\chi(z) = \varepsilon\varphi(x)\chi(z). \qquad (4.3)$$

As we can see from Eq. (4.3) the potential $V(z)$ is additive. The motion along z is not disturbed by the present magnetic field. Thus the z-part of the final solution will remain the same as before and the corresponding energy of the 1D bound state will be added. The x-part of the Eq. (4.3) is the Schrödinger equation for a one-dimensional harmonic oscillator of frequency $\omega_C = |q|B/m$ (so called cyclotron frequency) with the center at $x_0 = \hbar k_y/qB$. The wavefunction $\varphi(x)$ can be written in form of Hermite polynomials, [1]. The contribution to the total energy from the harmonic oscillator is

$$E_n^B = \hbar\omega_C(n + 1/2), n \in \mathbb{N}, \qquad (4.4)$$

where $\mathbb{N}$ denotes the set of non-negative integers. The energy E_n^B does not depend on k_y. Thus states with given n but different k_y are degenerate forming so called *Landau levels*.

The originally constant density of states for 2D quantum system changes due to presence of perpendicular magnetic field. It collapses to a series of δ-functions at given energies E_n^B spaced from each other by quantity $\hbar\omega_C$ (in an ideal case where electrons are never scattered). Usually it is assumed that δ-functions are broadened to a Gaussian or Lorentzian profile. The allowed number of states in each Landau level per unit area is given by an equation (the spin degeneracy is already included)

$$n_B = \frac{|q|B}{\pi\hbar}. \qquad (4.5)$$

With increasing magnetic field B the separation between the Landau levels grows. So does the number of states n_B each Landau level can hold.

4.2 Parallel magnetic field

To get an in-plane magnetic field $\vec{B} = (0, B, 0)$ one can choose the vector potential gauge in a form $\vec{A} = (Bz, 0, 0)$. The corresponding Hamiltonian of the system is

$$\mathcal{H} = \frac{p_x^2}{2m} + \frac{(qBz)^2}{2m} + \frac{p_y^2}{2m} - \frac{qBp_xz}{m} + \frac{p_z^2}{2m} + V(z). \qquad (4.6)$$

The associated Schrödinger equation can be solved either with the help of the standard perturbation theory or with the help of the tight binding approximation (TBA) introduced above. We will use the TBA procedure and the same notation as we did in Subsection 2.2.1 and in Section 3.2. The form of the Hamiltonian allows the separation of variables. The x, y-dependent part of the eigenstates are plane waves with the 2D wavevector $\vec{k} = (k_x, k_y)$. The remaining z-component of the eigenstates

is described with the wavefunctions $|\chi_\nu(z - z_i)\rangle$ of the isolated wells within the scope of TBA. We assume that these wavefunctions do not depend on magnetic field B and that $r = s = 0$ (s and r are the shift and overlap integrals defined earlier in Subsection 2.2.1). We express the influence of the magnetic field $\vec{B} = (0, B, 0)$ with the shift of the energy levels of the isolated quantum wells:

$$E_{R,L}(B) = E_{R,L}(B = 0) + \frac{\hbar^2(k_x - k_{R,L})^2}{2m_\parallel} + \frac{\hbar^2 k_y^2}{2m_\parallel}, \tag{4.7}$$

where $m_\parallel$ is the in-plane effective mass of the particle and $k_{R,L} = qBz_{R,L}/\hbar$. Generally the origin of coordinates can be chosen so that the equality $z_R = -z_L$ is fulfilled. In that case the parameter Δ (defined in Section 3.2) is given by expression $\Delta = 2z_R = -2z_L$.

Using the last equation for energy states of isolated wells and the orthonormality of states $|\chi_\nu(z - z_i)\rangle$ (used as a basis set) we can write the Hamiltonian of the system in a matrix form

$$\mathcal{H} = \begin{bmatrix} E_L(B) & t \\ t & E_R(B) \end{bmatrix}, \tag{4.8}$$

where t is the transfer integral defined in Subsection 2.2.1. The formula for eigenenergies follows

$$E_{1,2} = \frac{E_R + E_L}{2} \mp \sqrt{\frac{(E_R - E_L)^2}{4} + t^2}, \tag{4.9}$$

where index 1 (2) belongs to sign - (+), respectively. The eigenfunctions are again the linear combinations of states $|\chi_\nu(z - z_i)\rangle$. Entering Eq. (4.7) into (4.9) we obtain:

$$E_{1,2}(k_x, k_y) = \frac{E_L(0) + E_R(0)}{2} + \frac{\hbar^2(k_x^2 + k_y^2)}{2m_\parallel} + \frac{q^2 B^2 \Delta^2}{8m_\parallel}$$
$$\mp \sqrt{\frac{1}{4}\left(E_R(0) - E_L(0) - \frac{\hbar qB\Delta}{m_\parallel}k_x\right)^2 + t^2}. \tag{4.10}$$

We can see that the magnetic field applied along y axis modifies the energy dispersion along x axis.

4.2.1 Indirect excitons in in-plane magnetic field

Indirect excitons (IX) being formed in the tilted DQW under applied bias voltage have attracted attention in the theoretical and experimental field during last years. The excitonic photoluminescence (PL) in DQW was theoretically studied by Gorbatsevich and Tokatly, see [5] and later on also by Chang and Peeters, [6]. We present here just the basic overview of this topic.

The spatial separation of electrons and holes in adjacent wells leads in the in-plane magnetic field $B_\parallel$ to a shift of the IX ground state from the zero point of

the reciprocal space to a finite center-of-mass (CM) momentum in the reciprocal space. The exciton in-plane dispersion remains parabolic, but its minimum is displaced. The IX dispersion at a finite $\vec{B}_\parallel = (0, B_\parallel, 0)$ can be written in following approximative form:

$$E_{IX}(P_x, P_y) = E_0 + \frac{P_y^2}{2M} + \frac{(P_x - |e|B_\parallel \Delta)^2}{2M}, \qquad (4.11)$$

where Δ denotes the main distance between an electron and a hole forming IX, E_0 and M mark the IX energy at rest and its in-plane mass, respectively. P_x and P_y are the in-plane components of the IX momentum. From Eq. (4.11) we see that the displacement of parabola is linear in magnetic field $B_\parallel$ and also in parameter Δ.

Only the IX with nearly zero momentum $\vec{P} \approx \vec{0}$ can be optically active due to the conservation of the particle's momentum (the slight relaxation of the momentum conservation appears due to the finite photon momentum). The optically generated excitons relax to the states close to the new dispersion minimum $\vec{P} = (|e|B_\parallel \Delta, 0, 0)$. Because their new momentum is not zero the IX are optically inactive. So there should be almost no PL arising from IX in the higher in-plane magnetic fields. The only signal we get is from carriers thermally excited to states with higher energies, which explains the blueshift of the IX peak.

Parlangeli *et al.* introduced in [7] a simple model of IX PL in the in-plane magnetic field $B_\parallel$, using also the formula (4.11). They made few other assumptions: they used the Boltzmann statistics of the IX gas instead of the Bose-Einstein distribution and assumed a constant density of the IX gas. Finally they obtained the formula for PL intensity arising from optically active states

$$I \propto exp\left(-\frac{e^2 \Delta^2 B_\parallel^2}{2M k_B T}\right), \qquad (4.12)$$

where k_B denotes the Boltzmann constant and T is standard symbol for the temperature of IX gas. As outcome we see that the energy of PL line should increase quadratically with $B_\parallel$.

4.2.2 Brief overview of published experimental results

Parlangeli *et al.* published in 2000 their measurements of IX PL of DQWs in the system GaAs/AlGaAs in the in-plane magnetic field, [8]. They applied previously introduced model of the Gaussian damping to explain measured data. A very good agreement between theory and experiment was achieved. They observed the quadratic increase of the IX recombination energy with increasing $B_\parallel$. The damping of IX PL peak was as well in accordance with theory, in particular with Eq. (4.12).

Another experiment was performed by Butov *et al.*, [9]. They studied the kinetics of IX PL at a finite $B_\parallel$. They showed the expected quadratic shift of IX PL energy

as well as the damping of the IX PL line. However, their damping was substantially slower with $B_\parallel$ than Parlangeli *et al.* observed.

The recent experiments performed by our group are in contradiction to the above mentioned theory and confirmation experiments, see [10, 11]. The IX line did survive in the PL spectra of studied DQW structure up to high in-plane magnetic fields. The total PL intensity of IXs remained unchanged or slightly decreased, but no Gaussian damping was found. Orlita *et al.* explain in [11] the survival of the IX line by the IX localization which enables the relaxation of the IX in-plane momentum, whose conservation is responsible for the damping of the IX luminescence intensity observed by other groups. This localization should be supported by a relatively weak non-radiative recombination in comparison to the radiative one observed in the studied DQW structure.

To conclude, the above presented measurements demonstrate that there is a strong dependence of IX PL on specific parameters of samples like the exciton density, the presence of localization centres, etc.

4.2.3 Density of states

With the knowledge of the energy position $E_i(k_x, k_y)$ we are able to write down the formula for density of states $g(E)$ on the given energy E (the spin degeneracy is already included)

$$g(E) = \frac{2}{(2\pi)^2} \sum_{i=1,2} \int_{1.BZ} \delta(E_i(k_x, k_y) - E) dk_x dk_y, \qquad (4.13)$$

where 1.BZ states for the first Brillouin zone. Further reading to this topic can be found for example in [4].

Chapter 5

Landé g-factor

The changes (shifts and splittings) of the energy spectra of a particle or an atom due to the presence of an external magnetic field are called *Zeeman effects*. The study of Zeeman splittings and magnetic g-factors of free electrons, holes and bound complexes such as exciton and trion can give us some information about the binding energy of bound complexes, coupling between exciton states, etc. It is also relevant for other phenomena. In this chapter we present a corresponding basic theory of Zeeman splitting for an atom, an electron and a hole as well as for the bound complexes in GaAs/AlGaAs.

5.1   Zeeman splitting in an atom

In most atoms there are several electron configurations (given by a set of quantum numbers) giving the same energy, the energy levels are degenerate. The presence of a magnetic field breaks the degeneracy resulting in the separated energy levels for each electron configuration.

The Hamiltonian of an atom in a magnetic field is:

$$\mathcal{H} = \mathcal{H}_0 + \mathcal{W}, \tag{5.1}$$

where $\mathcal{H}_0$ is the unperturbed Hamiltonian of the atom (without magnetic field) and perturbation $\mathcal{W}$ can be written in the following form

$$\mathcal{W} = i\frac{|e|\hbar}{m_0}\vec{A}\nabla - \frac{|e|\hbar}{2m_0}\vec{\sigma}\cdot\vec{B}, \tag{5.2}$$

where m_0 is the reduced mass and $-|e|$ is the charge of an electron, $\hbar$ is reduced Planck constant. The operator $\vec{\sigma}$ is related to the spin angular momentum $\vec{s}$ of an electron. This relation is given by equation $\vec{s} = \frac{1}{2}\vec{\sigma}$. Note that we neglected the term proportional to A^2 arising from expansion of $(\vec{p} - e\vec{A})^2$.

Putting the formula $\vec{A} = 1/2[\vec{B} \times \vec{r}]$ into expression for $\mathcal{W}$ and using the definition of an orbital angular momentum $\vec{L}$ ($\vec{L} = \vec{r} \times (-i\hbar\nabla)$) Eq. (5.2) can be rewritten

into

$$\mathcal{W} = -\frac{|e|}{2m_0}(\vec{L} + 2\vec{s}) \cdot \vec{B} = -\vec{\mu} \cdot \vec{B}. \tag{5.3}$$

We introduced $\vec{\mu}$, so called operator of magnetic momentum of an electron

$$\vec{\mu} = \frac{e}{2m_0}(\vec{L} + 2\vec{s}). \tag{5.4}$$

To simplify the later algebra we define the total angular momentum $\vec{J}$ by

$$\vec{J} = \vec{L} + \vec{s}. \tag{5.5}$$

We treat our Hamiltonian $\mathcal{H} = \mathcal{H}_0 - \vec{\mu} \cdot \vec{B}$ in sense of the standard perturbation theory. First of all we need to describe unperturbed eigenstates of an atom, we do so with the help of a set of quantum numbers $|njlm\rangle$. We use the standard notation of quantum mechanics which can be widely found in the literature, e.g. in [12, 13].

Now our task is to evaluate the matrix element of perturbation $\mathcal{W}$ using the eigenstates $|njlm\rangle$,

$$\langle njl'm'| - \vec{\mu} \cdot \vec{B}|njlm\rangle. \tag{5.6}$$

To evaluate it we rewrite the expression for operator of magnetic moment of an electron $\vec{\mu}$ with the help of Eq. (5.5)

$$\vec{\mu} = \frac{|e|}{2m_0}(\vec{L} + \vec{s} + \vec{s}) = \frac{|e|}{2m_0}(\vec{J} + \vec{s}) = \widehat{G}\vec{J}, \tag{5.7}$$

where we introduced new operator $\widehat{G}$. To express this operator we make a scalar product of Eq. (5.7) with vector $\vec{J}$. We obtain

$$\widehat{G} = \frac{|e|}{2m_0}\left(1 + \frac{\vec{J}^2 + \vec{s}^2 - \vec{L}^2}{2\vec{J}^2}\right), \tag{5.8}$$

where we used the square of the Eq. (5.5).

Furthermore we use the action of operators $\vec{J}^2, \vec{s}^2, \vec{L}^2, \vec{J}_z$ on the eigenfunction $|njlm\rangle$ which can be found in [12, 13]. The magnetic field $\vec{B}$ in the perturbation term does not depend on coordinates, Eq. (5.3). Therefore we reduce our calculation and evaluate the effect of perturbation $\mathcal{W}$ in following form (the magnetic field $\vec{B} = (0, 0, B)$ is parallel to the z axis):

$$\langle njl'm'| - \mu_z B|njlm\rangle = \langle njl'm'| - \widehat{G}J_z B|njlm\rangle$$
$$= -\mu_B\left(1 + \frac{j(j+1) + s(s+1) - l(l+1)}{2j(j+1)}\right)mB\delta_{mm'}\delta_{ll'}. \tag{5.9}$$

For the sake of brevity so called Bohr magneton appears in the last equation, $\mu_B = \frac{|e|\hbar}{2m_0}$. There are following values of quantum numbers for electrons: $s = 1/2$, $j =$

$|l \pm 1/2|$, $l = 0, 1, 2, \ldots$, $m = \pm j, \pm(j-1), \ldots$ To simplify the last formula so called *Landé g-factor* is defined:

$$g = 1 + \frac{j(j+1) + s(s+1) - l(l+1)}{2j(j+1)}. \tag{5.10}$$

The energy of a level $E_{n,j}$ in the presence of magnetic field is given by

$$E_{n,j,l,m} = E_{n,j} - mg\mu_B B. \tag{5.11}$$

The shifts of energy levels in the presence of magnetic field are symmetric to the unperturbed value $E_{n,j}$. The difference between adjacent energy levels is given by

$$\Delta E = g\mu_B B, \tag{5.12}$$

and it is proportional to the Langé g-factor and to the induction of magnetic field. The splitting described by Eq. (5.12) is called *anomalous Zeeman effect*. It was observed experimentally before spin of an electron was theoretically discovered and therefore a satisfactory explanation of this effect was missing.

In case of a spinless particle the Landé g-factor has value $g = 1$ and the distance of adjacent energy level is for all states the same

$$\Delta E = \mu_B B. \tag{5.13}$$

The splitting of energy levels given by Eq. (5.13) is known as *normal Zeeman effect*.

In case of strong applied magnetic fields[1] the coupling between orbital and spin angular momentum is broken and each of them shows an independent reaction to the magnetic field. The perturbation $\mathcal{W}$ in this case can be written

$$\mathcal{W} = -\vec{\mu} \cdot \vec{B} = -\frac{|e|B}{2m_0}(\vec{L_z} + 2\vec{s_z}). \tag{5.14}$$

As unperturbed wavefunctions we choose $|nlm_l m_s\rangle$. m_l (m_s) denote the projection of the orbital (spin) angular momentum into the z axis, respectively. The correction to the energy due to the presence of strong magnetic field is given by

$$\Delta E_{m_l, m_s} = -\mu_B B(m_l + 2m_s). \tag{5.15}$$

The distance of adjacent splitted components is $\mu_B B$. The splitting of energy levels in strong magnetic fields described by Eq. (5.15) is called *the Paschen-Back effect*.

5.2 Landé g-factors of the electron and hole in GaAs/AlGaAs

Zeeman splitting, Landé g-factor and their dependencies on the well thickness L and on the magnetic field have been investigated by many groups in GaAs/AlGaAs

---

[1] The splitting ΔE is greater than the doublet splitting of an level induced by magnetic field.

type I and II quantum wells during last years. The analysis of measured spectra is provided using the spin Hamiltonian formalism, mostly.

We consider first the Hamiltonian for bulk excitons. They consist of an electron associated with the conduction band minimum and of a hole associated to the valence band maximum. Van Kesteren *et al.* derived in [14] the Hamiltonian of a system using symmetry considerations only[2]

$$\mathcal{H}_{ex} = \mathcal{H}_e + \mathcal{H}_h + \mathcal{H}_{e-h}, \tag{5.16}$$

where

$$\mathcal{H}_e = \mu_B g_e \sum_{i=x,y,z} S_{e,i} B_i \tag{5.17}$$

$$\mathcal{H}_h = -2\mu_B \sum_{i=x,y,z} (\kappa J_{h,i} + q J_{h,i}^3) B_i \tag{5.18}$$

are terms describing the Zeeman splitting of the electron and hole in the presence of magnetic field, respectively, and term

$$\mathcal{H}_{e-h} = -\sum_{i=x,y,z} (a J_{h,i} S_{e,i} + b J_{h,i}^3 S_{e,i}) \tag{5.19}$$

describes the spin-spin coupling of the electron and hole forming an exciton. The cubic terms of $J_{h,i}^3$ are mostly much smaller than the linear ones and can usually be neglected in calculations. The explanation of used parameters follows:

- μ_B is the Bohr magneton,

- g_e is Landé g-factor of the electrons,

- κ and q are the Luttinger constants for the hole,

- a,b are the spin-spin coupling constants.

In GaAs/AlGaAs QWs the upper valence band is split into a light-hole band with $J_{h,z} = \pm 1/2$ and a heavy-hole band with $J_{h,z} = \pm 3/2$. At low temperatures the hole occupies the $J_{h,z} = \pm 3/2$ states predominantly. We assume, in accordance with [15], that for the valence band the separation of heavy- and light-hole states is much larger than any Zeeman splitting. To describe the sublevels of the heavy-hole band we use an effective spin $\Sigma_z = \pm 1/2$. Under all these assumptions and neglecting spin-spin coupling the Zeeman splitting of the electron and hole is given by

$$\mathcal{H}_e + \mathcal{H}_h = g_e \mu_B \vec{B} \cdot \vec{S} - g_h \mu_B B_z \Sigma_z. \tag{5.20}$$

g_h can be expressed in terms of Luttinger parameters

$$g_h = 6\kappa + 13.5q. \tag{5.21}$$

---

[2]Therefore it is valid also for type I and II GaAs/AlGaAs quantum wells.

5.2.1 The summary of published experimental results

Different experimental methods were used to determine the sign and the value of Landé g-factors of the electron and hole. Some results were obtained already but not all of them are in the mutual agreement. We try to summarize recent work in this field in next paragraphs.

Van Kesteren *et al.* published in 1990 their work where they studied the excitons in type II GaAs/AlAs QWs using optically detected magnetic resonance in zero and in a finite magnetic fields, [14]. The substrate and cap were from GaAs, the inside structure consisted of GaAs and AlAs layers. More samples with different widths of GaAs and AlAs layers were studied. For Landé g-factor of the electron they found out following values: $g_{e,x} = g_{e,y} \doteq (1.97 - 1.98)$; $g_{e,z} \doteq 1.9$ which remained the same for all samples. The results for the hole g-factor depend on the particular sample: $g_{h,x} = g_{h,y} < 0.01$; $g_{h,z} = 2.3$ (for 2.5 nm GaAs layers); $g_{h,z} = 2.9$ (for 1.7 nm GaAs layers). Van Kesteren *et al.* made the conclusion that the dependence of the hole g value on the thickness of the GaAs layer is probably due to the valence band mixing in the QWs.

The study of the magnitude and sign of the g-factor for conduction electrons in type I GaAs/AlGaAs QWs was done by Snelling *et al.* in 1991, [16]. This group used the combined measurement of decay time of PL and of the suppression of its circular polarization under polarized optical pumping. Experimentally determined values of g_e as well as theoretically calculated ones are investigated with respect to the well width. In theoretical calculations the 3-band $\vec{k} \cdot \vec{p}$ theory was used together with the assumption of allowance for non-parabolicity of the bulk GaAs conduction band and penetration of the electronic wavefunctions into the AlGaAs barrier. The barrier Al content was 0.3. However, they found out that the penetration effect is rather small for $L \geq 5$ nm.
For $L < 5$ nm the electron is expected to spend much of its time in the barrier and therefore its g value should become positive, reaching the AlGaAs bulk value $\sim +0.4$ for $L \to 0$ nm. With increasing well width ($L \geq 5$ nm) the g value is expected to approach monotonously the asymptotic value of bulk GaAs $\sim$ -0.44. So g_e should reverse the sign and cross zero axis around $L \doteq 5$ nm.

Snelling *et al.* published another paper in 1992 where besides the electron g-factor the exciton and heavy-hole g-factor in type I GaAs/AlGaAs QWs were investigated, [15]. The barrier content was 0.36. This time they collected the exciton PL from their sample using the polarizer to distinguish between the opposite circular polarizations, σ^+ and σ^-. The exciton g-factor g_{ex} was derived from their measurements and using equation $g_{ex} = g_e + g_h$ the hole g-factor was calculated (as g_e the above mentioned reference was used). With increasing well width L the hole g-factor also increases, from negative values for small L ($L < 8$ nm) it becomes positive for large L ($L > 8$ nm). Because the theoretical calculations using Eq. (5.21) and constant parameters κ and q do not reproduce the observed L dependence of g_h Snelling *et al.* conclude that Luttinger parameters κ and q may vary with L as

well.

In 1996, Shields *et al.*, [17], investigated the magnetooptical spectra of neutral and negatively charged excitons in remotely doped 30 nm-wide GaAs QWs upon their excess electron density. At this moment we point out just the result of g_e measurement: $g_e \doteq (0.42 \pm 0.02)$ which is in a very good agreement with the bulk value of GaAs $\sim$ -0.44 (apart from the sign which is always a little bit controversial because it depends on sign convention used during computation).

The dependence of electron g-factor on the total density of the two-dimensional electron system (2DES) was measured by Tutuc *et al.* in 2002, see [18], using Shubnikov-de-Haas oscillations and in-plane magnetoresistance. They assumed g as independent of the applied magnetic field. Their measurements were done by the field at which full spin polarization was achieved. The values of measured electron g-factor vary from 1.3 (total density of 2DES 0.8×10^{10} cm^{-2}) up to 2.6 ($n = 6.5 \times 10^{10}$ cm^{-2}). This is in contradiction with latest theory as this predicts that with decreasing density of the 2DES the g-factor should monotonically increase. Tutuc *et al.* suppose that it is due to the low disorder GaAs 2D electrons and holes.

One of the latest reports to this topic we found is the temperature dependence of the conductivity and the magnetoresistance in parallel field of a high mobility 2DHG in GaAs/AlGaAs heterostructure which was measured by Proskuryakov *et al.* in 2002, see [19]. The output of their measurements is the dependence of magnetic hole g-factor on the hole density counted in accordance with the formula $g = (2E_F)/(\mu_B B_S)$, where B_S is the magnetic field corresponding to the full spin polarization of the 2D system. They observed a linear behavior, increasing the hole density the hole g-factor also increases, varying from value 0.4 for 1.5×10^{10} cm^{-2} up to 1.45 for hole density 8.2×10^{10} cm^{-2}.

5.3 Landé g-factor of the exciton in GaAs/AlGaAs

A neutral exciton X_0 consists of one conduction-band electron and one valence-band hole bound by the Coulomb interaction. We consider the heavy-hole band only which is consistent with previous section. There are four basis states $|S_z, J_{h,z}\rangle$ for such a formed exciton:

$$e \uparrow h \downarrow; \quad e \downarrow h \uparrow; \quad e \uparrow h \uparrow; \quad e \downarrow h \downarrow. \tag{5.22}$$

In zero field there are two doublets in which spins are parallel and antiparalell. In a magnetic field applied parallel to the z axis there are further splittings of the doublets. As we know from the selection rules only transitions with the total spin change of ± 1 are optically allowed. Total spin change of +1 (-1) corresponds to right- (left-) handed circularly-polarized PL light indicated by a solid (dotted) arrow in Fig. 5.1. As we can see only two optically allowed transition are observable. The corresponding splitting is given by [15]

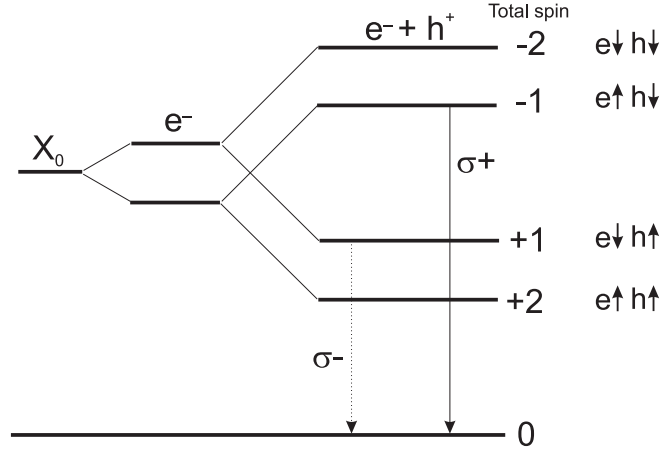$$\Delta_{1,2} = |g_e + g_h| \mu_B B_z. \tag{5.23}$$

Figure 5.1: The energy level diagram of the neutral exciton with two optically allowed PL transitions. After reference [20].

According to the Snelling *et al.* the value of the exciton g-factor can be determined using g_e and g_h values

$$g_{ex} = g_e + g_h. \tag{5.24}$$

Since it is not possible to make an experimental distinction between the electron and hole g-factors by using PL, the expression $g_e + g_h$ is often labeled as an effective exciton g-factor g_{eff} resulting in a splitting $\Delta E = g_{eff}\mu_B B$.

As described already in Subsection 5.2.1 the exciton g factor was measured in 1992 by Snelling *et al.*, [15]. The dependence of g_{ex} on the well width L was investigated. They observed the change of sign for L between 7.34 nm and 11.2 nm. They made a conclusion that g_{ex} is negative for narrow wells and increases monotonically together with the well width.

Recently the dependence of the exciton g-factor on the magnetic field (from 0 to 9 T) was studied by Glasberg *et al.* in PL spectra of GaAs/AlGaAs QWs, [21]. The value of $\sim +0.5$ was found for g_{ex} at very low fields. For higher fields there is the sign reversal and last reported value is ~ -0.7 for magnetic field slightly above 7 T.

To demonstrate the fact that exciton g-factor and Zeeman splitting still attract the attention of scientific world we report about PL measurement in magnetic fields up to 50 T in different GaAs/AlGaAs QW samples published by Vanhoucke *et al.* in 2001, [20]. The value $g_{ex} = 1.5$ for 10 nm wide QW was reported. However this work did not confirm the previous conclusion about magnetic field dependence of g_{ex}. Vanhoucke *et al.* conclude that g_{ex} does not depend on the magnetic field.
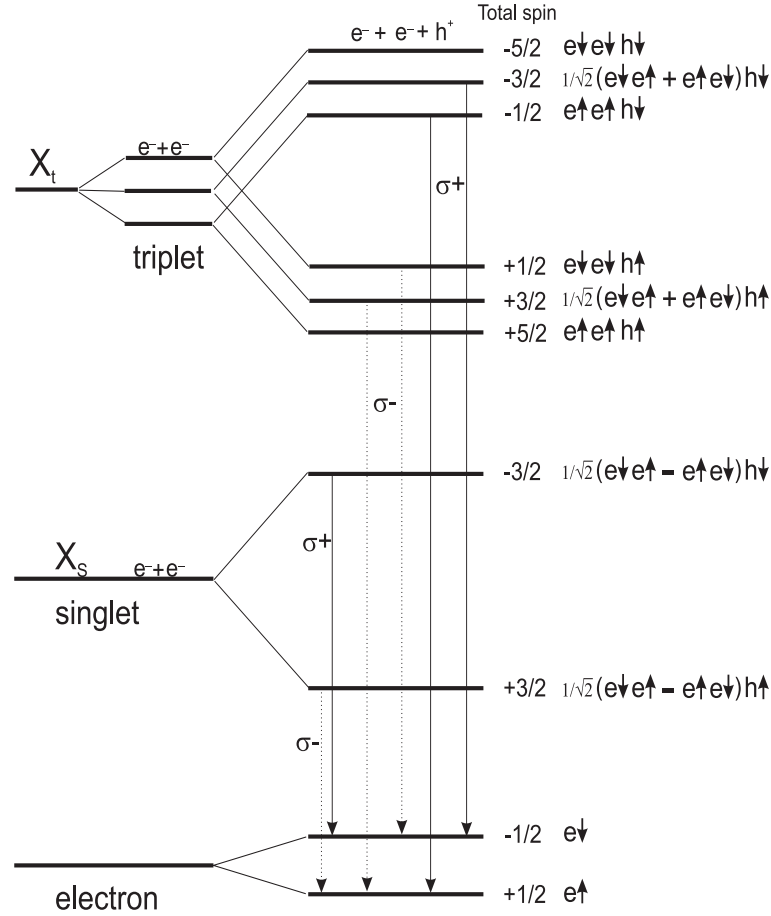
Figure 5.2: The energy level diagram of the triplet and singlet state of the negatively charged exciton with six optically allowed PL transitions. After reference [20].

5.4   Landé g-factors of the charged excitons in GaAs/AlGaAs

Charged excitons (also called trions) are expected to form when neutral excitons are present in an environment with excess holes or electrons. The negatively (positively) charged exciton, often labeled as X^- (X^+), emerges when a third particle, an electron (a hole), is bound to the neutral exciton, respectively. We will outline some basic knowledge about trions, especially for negatively charged excitons. The similar conclusion can be made also for positively charged excitons.

Since the two electrons forming X^- are identical the well known Pauli's exclusion principle allows only an antisymmetric total wavefunction. So we can factorize it into symmetrical (antisymmetrical) spin part with an antisymmetrical (symmetrical) space part, respectively. There is one possibility how to construct the antisymmetrical spin wavefunction of two electrons, known as the singlet state X_s^-, $1/\sqrt{2}(e \downarrow e \uparrow - e \uparrow e \downarrow)$. There are three possibilities how to construct the symmetrical spin wavefunction, known as the triplet state X_t^- (can be found in Fig. 5.2).

These states are degenerate, the degeneracy is removed in the presence of magnetic field due to the Zeeman interaction determined by trion g-factor. In Fig. 5.2 we consider the interaction of conduction band electrons (spin $\pm 1/2$) and heavy-holes (spin $\pm 3/2$) only. The recombination of one electron and the hole can be observed leaving one excess electron in the QW. There are in total eight different energy levels for X^- but only six of them are optically allowed due to the selection rules.

As total spin of the two electrons in singlet state is equal to zero the Zeeman splitting is determined by the spin of the hole and hole g-factor only. However, both transitions from the singlet level differ from each other in the final state of an electron, consequently in spin projection of the final electron. Therefore the electron g-factor has to be taken into account while determining the Zeeman splitting of X_s^- as well. For the triplet state it is clearly seen that both g-factors (g_e and g_h) play a significant role. The observable Zeeman splitting is after Vanhoucke et al. given by equation

$$\Delta E = (g_e + 3g_h)\mu_B B. \tag{5.25}$$

As mentioned before the straight determination of g_e and g_h is not possible from PL spectra. Consequently the effective g-factor of negatively (positively) charged exciton g_{X-} (g_{X+}), respectively can be defined by

$$\Delta E = g_{X\pm}\mu_B B. \tag{5.26}$$

As ΔE usually the difference in PL energy between the σ^+ and σ^- component of the singlet and triplet state is used.

The PL arising from the triplet states of charged excitons is observable in strong magnetic fields. In our experimental results we deal with the PL arising from the singlet state of charged excitons only.

The formation of both, singlet and triplet state of X^- was observed by Shields et al. already in 1996, [17]. The evolution of PL peak energies with magnetic field was investigated in remotely doped 30 nm-wide GaAs/AlGaAs QWs, nevertheless, no particular value of $g_{X\pm}$ was pointed out from their experiments.

One of the first values for g_{X-} and g_{X+} were determined by Glasberg et al. using the PL measurement in magnetic fields 0 to 9 T in GaAs/AlGaAs QWs, [21]. Changing the illumination conditions they were able to control the density and type of the excess carriers in the QW. Consequently they could resolve the PL arising from the recombination of X^- and X^+ within the same sample. They observed a magnetic field dependence of the g-factors g_{X-} and g_{X+}, especially for g_{X+}. Both g-factors show the positive sign and roughly the same value $\sim +0.5$ at low field and sign reversal after. With increasing the magnetic field the g-factors decrease monotonically, reaching values slightly below -1 for $g_{X_s^-}$, below -2 for $g_{X_s^+}$ at approximately 7 T.

In one of the latest measurements of PL in magnetic fields up to 50 T in different GaAs/AlGaAs QW samples Vanhoucke et al. distinguished the singlet and triplet states of X^- trion, [20]. They outlined below mentioned effective g-factors of X^-

trion for three different QW widths: 15 nm: $g_{X_s^-} = 1.3$, $g_{X_t^-} = 1.4$; 12 nm: $g_{X_s^-} = 1.9$, $g_{X_t^-} = 2.1$; 10 nm: $g_{X^-} = 1.9$ (as there was no experimental recognition of different states of X^- in this QW). Furthermore Vanhoucke *et al.* conclude that g_{X^-} and g_{X^+} do not depend on the magnetic field which is again in contradiction with Glasberg's measurements.

As we could see from the overview many special structures were designed to study and enhance particular effects. A year ago a new sample consisting of a double-barrier resonant tunneling diode RTD where the GaAs QW was embedded between AlAs barrier was introduced by Teran *et al.*, [22]. By varying the applied bias and the intensity of illumination they were able to observe both, the negatively and positively charged excitons. The formation of trions and their binding energy was discussed. However, no particular value of $g_{X^\pm}$ was pointed out from their experiments.

Chapter 6

Experimental details

6.1 Experimental setup

Our measurements of PL in electric and magnetic fields were realized in the optical laboratory, Department of Semiconductors and Semiconductor Optoelectronics of the Institute of Physics, Charles University in Prague. The basic scheme of our experimental setup is sketched in Fig. 6.1. We used the standard configuration where the excitation photon energy exceeds the band gap of $Al_xGa_{1-x}As$, so carriers are supplied into the quantum wells by diffusion and drift from the surroundings barriers. Luminescence was excited by a 25 mW semiconductor diode laser ($\lambda = 633$ nm). We suppose that the excitation intensity per unit area is $I_0 \approx 10$ Wcm^{-2} after the focusing of laser beam on the sample. This excitation density was lowered by the neutral density filters. The PL was measured by a commercial FT-IR spectrometer. The structure of our sample allowed us to apply a bias voltage U_{nn} by means of selective Ohmic contacts.

The measured sample was mounted into the cryostat of the superconducting magnet Spectromag SM4000-11.5 Oxford Instruments. It allows us to measure PL in the Faraday as well as in the Voigt configuration. The achievable magnetic field varies within the interval 0 - 11.5 T, however, for below reported measurements 9.6 T was the highest value we used. We can also vary the temperature inside the cryostat within the interval $\sim$1.4 - 300 K. The temperature is measured by resistors Allan-Bradley. Our experimental setup was supplemented with the new power supply from Oxford Instruments this year. It simplifies the control over the adjustment of the given value of magnetic field and increases the safety of operation in the laboratory.

The commercial Fourier spectrometer brand name IFS 66/S BRUKER was used to analyze the measured data. The PL of DQW was detected by the Si diode. The measured interval was 10000 - 14000 cm^{-1}, (1.24 - 1.74 eV). The standard spectral resolution, 2 cm^{-1} (0.25 meV), was used.
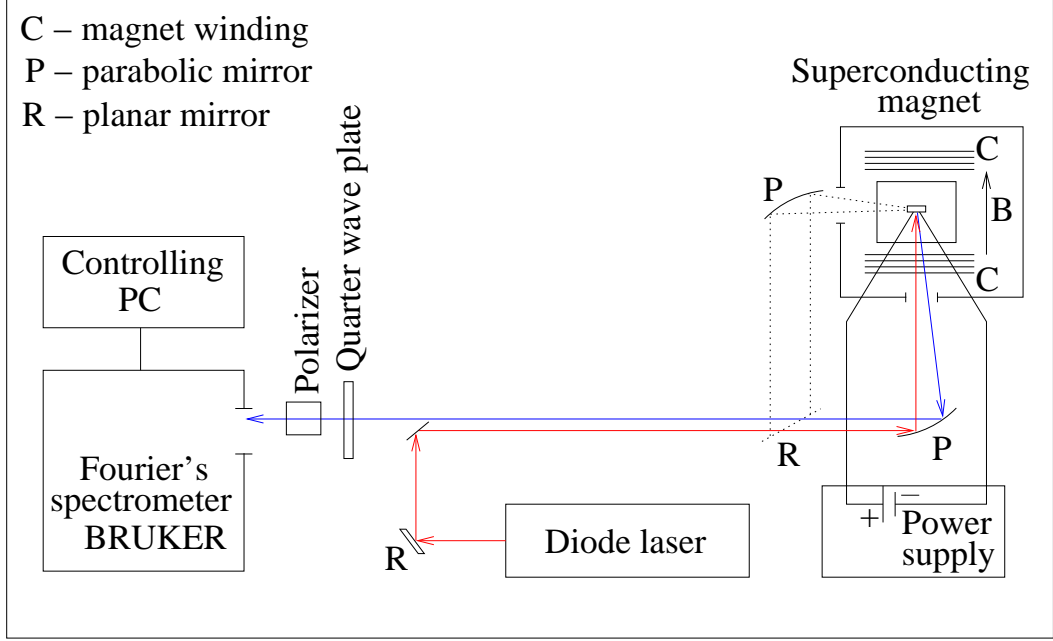
Figure 6.1: The basic scheme of our experimental setup for measurements of electro- and magneto-photoluminescence.

6.2   Sample TP982

Our sample was prepared by the Institute of Technical Physics I of Friedrich-Alexander University in Erlangen, Germany (thereof the abbreviation TP in the name of the sample).

The schematic picture of studied sample is sketched in Fig. 6.2. It was grown by MBE (this technique was described in Subsection 2.3.1) at a temperature of $630\,°C$ on a semi-insulating GaAs substrate oriented in the [001] direction. The growth started with a 400 nm-wide n-doped (Si, 1×10^{18} cm^{-3}) GaAs layer, followed by a 200 nm-wide intrinsic Al$_{0.33}$Ga$_{0.67}$As layer. Next, a sequence of two symmetric DQWs with 14ML ($\approx$ 4 nm)-wide Al$_{0.33}$Ga$_{0.67}$As central barrier was grown. The well widths are 28 ML ($\approx$ 8 nm). The growth then continued with a 200 nm-wide intrinsic Al$_{0.33}$Ga$_{0.67}$As layer, followed by a 200 nm-wide n-doped (Si, 1×10^{18} cm^{-3}) GaAs cap layer. The measured devices were defined by photolithography, mesa-isolated and selectively contacted to the bottom and to the top n-region. The flat-band regime was achieved for $U_{nn} \sim +0.2$ V. The n-top (n-bottom) contact was connected to the high (low) contact of the voltage source, respectively. The possibility to vary U_{nn} within the interval -1.5 V up to +2.0 V allows us to tilt the DQW in both directions.

Initially we wanted to study two different mesa structures, B8 and B12. Unfortunately, the structure B12 did not show a good response to the applied bias and the quality of measured spectra was insufficient. Thus all below presented ex-
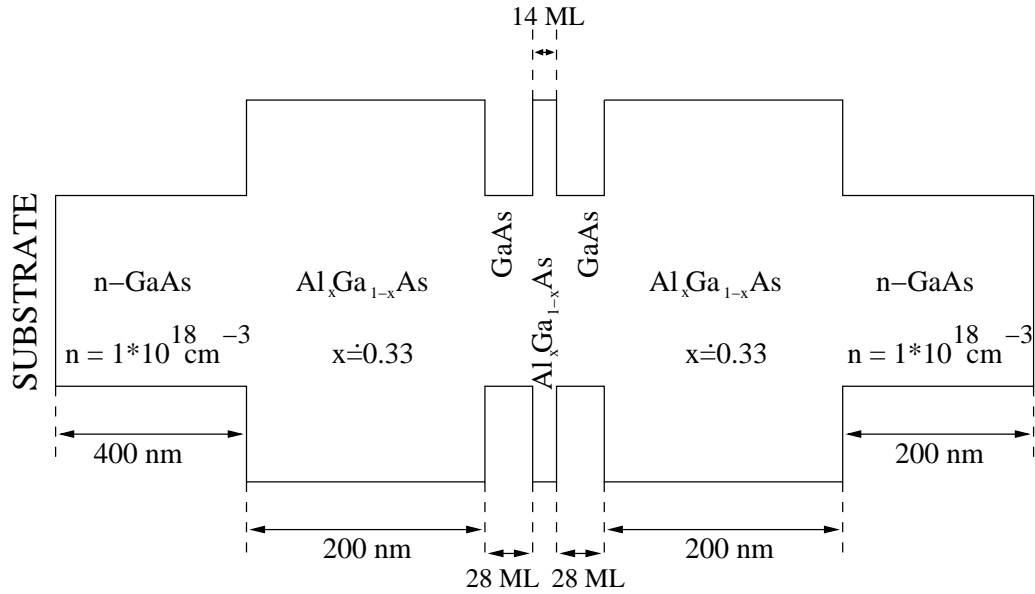
Figure 6.2: The schematic picture of studied sample TP982. The content of $Al_xGa_{1-x}As$ in the middle barrier is 0.33 as well. The unit ML denotes the monoatomic layer, 1 ML $\doteq$ 0.28 nm. Lengths are not in scale.

perimental results originate from the structure B8, sample TP982. The data were obtained within several measurements during my work on diploma thesis. Due to the readjustment of experimental setup it was not possible to keep all laboratory conditions identical for all measurements. Therefore, the spectra measured under the same conditions differ from each other slightly.

Chapter 7

Experimental results

7.1 Measurements without magnetic field

We start the presentation of our experimental results with the PL spectra of DQW in the zero magnetic field at $T = 5$ K. In Fig. 7.1 we can see the voltage dependence of PL from DQW. These spectra were chosen among all measured spectra at various temperatures as the sample ones to illustrate the basic features.

As introduced in Section 3.1 the direct (DX) and indirect (IX) transitions are clearly seen in Fig. 7.1. The inset in Fig. 7.1 is the schematic picture of the tilted DQW, shown to explain the nature of DX and IX transitions. Below the energy 1.53 eV we can see the slight increase in the PL intensity. This does not originate in the DQW. It is the background PL of the bulk GaAs (which was used as the substrate).

An immediately noticeable feature in Fig. 7.1 is a clear asymmetry of measured spectra with respect to the sign of U_{nn}. This effect is more pronounced in Fig. 7.2. It shows the voltage dependence of the peak energies deduced from spectra 7.1. As stated in the growth protocol described in Section 6.2 the sample TP982 was designed and grown as a symmetrical structure. Therefore, this asymmetry in PL spectra with applied bias voltage is a little bit unexpected. We assume that this asymmetry is induced by the damping of the excitation intensity in the sample as the number of photo-generated particles decreases exponentially with the penetration depth and by different effective thickness of the sample on sides of DQW where the light is absorbed. The absorption coefficient at the used excitation energy can be estimated as 2×10^4 cm^{-1} in GaAs and 10^4 cm^{-1} in AlGaAs. Since this penetration depth is comparable with the thickness of our sample, different density of electron-hole pairs is generated near the cap and the substrate layer.

In Fig. 7.1 we can see that under $U_{nn} = -0.7$ V more peaks than DX and IX can be resolved in PL of DQW. These peaks are labeled as A and B in accordance with Zvára *et al.* [23] where the explanation of these new bands was suggested. For the sake of completeness we will recall the basic assumptions and conclusions. As mentioned earlier the tilting of the DQW induced by the applied bias voltage
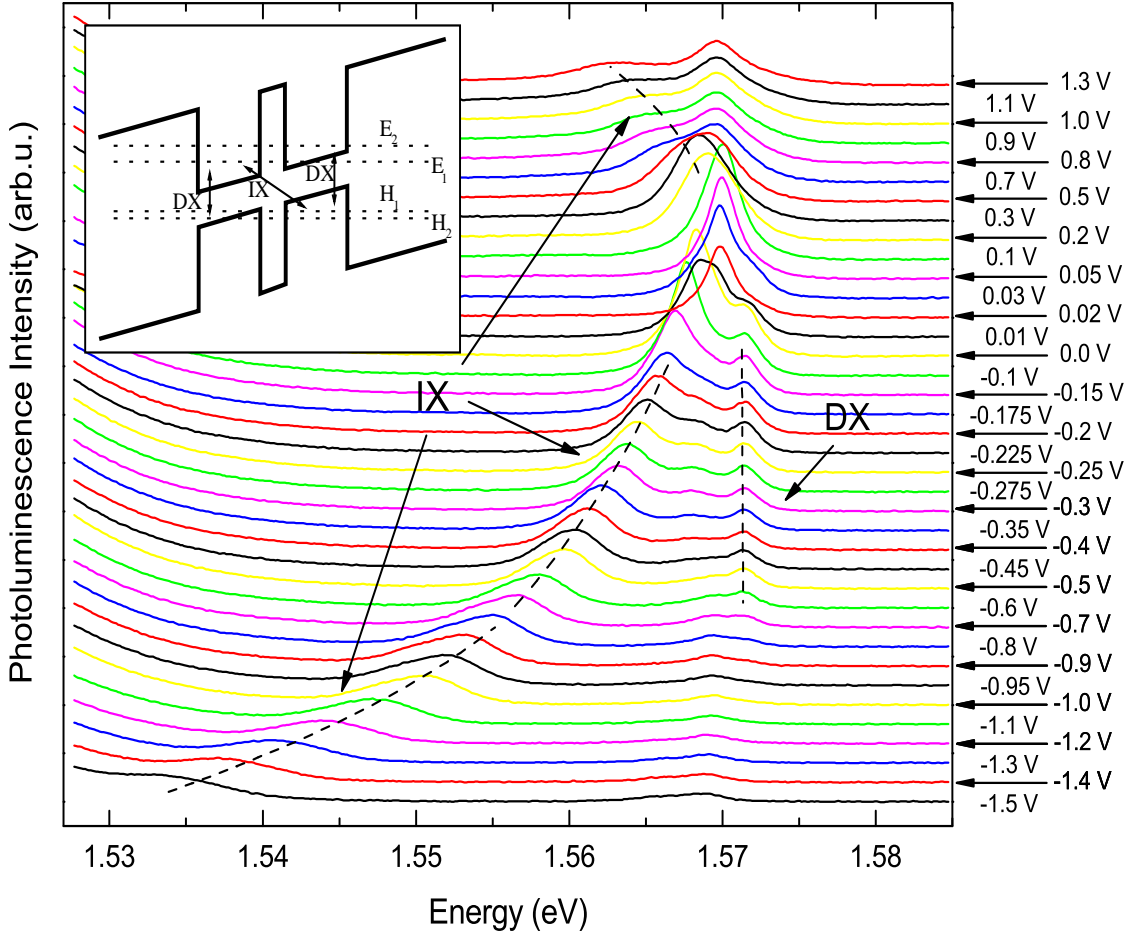
Figure 7.1: The PL spectra of DQW in the zero magnetic field, $T = 5$ K, excitation power $0.2I_0$. An apparent brake near $U_{nn} = -0.7$ V is caused by a non-equidistant step in the voltage. The black lines are just guides for eye. The inset shows the tilted DQW with schematically sketched DX and IX transitions.

leads to the localization of electrons and holes in the adjacent wells and to the screening of the external electric field. Both the electrons and the holes become degenerate in strong fields forming spatially separated two-dimensional hole (2DHG) and electron gases (2DEG). We assume that our structure is neutral and that the carrier density is less than 10^{11} cm^{-2} in our sample (it will be discussed below in this section). According to Zvára *et al.* such densities are insufficient to screen excitonic interaction efficiently, so our system should be described by excitons interacting with other free carriers.

The formation of A and B peaks is more visible in Fig. 7.3, especially for $U_{nn} = -0.5$ V and $U_{nn} = -0.7$ V. Both peaks are observed at a higher electric bias when 2D gases become degenerate. Due to the high density of electrons and holes in the respective wells the excitons interact with other quasi-particles, forming quasi-stable
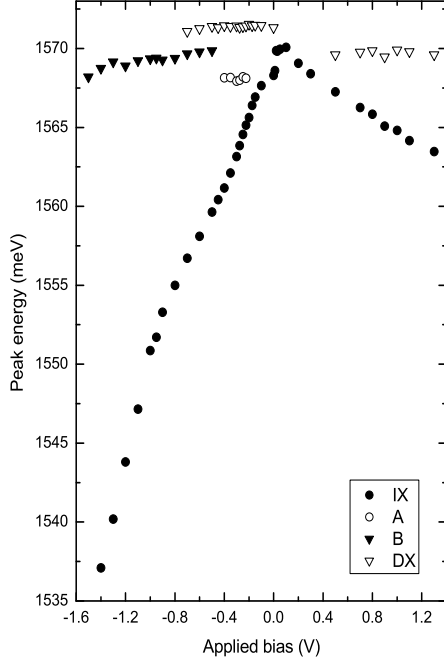
Figure 7.2: The voltage dependence of the peak energies in the zero magnetic field, $T = 5$ K, excitation power $0.2I_0$. The energies of peaks are deduced from Fig. 7.1.
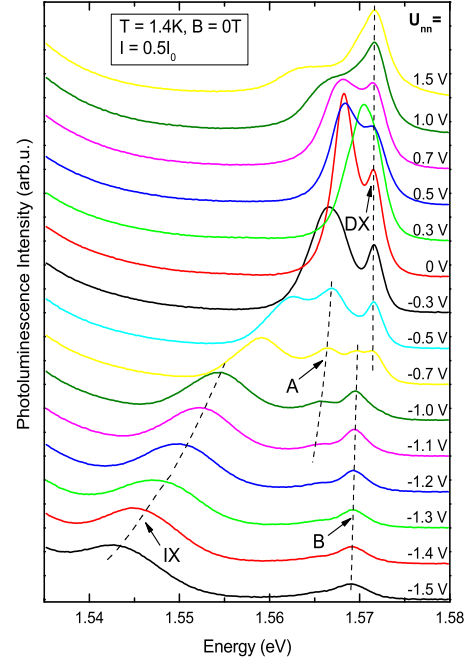
Figure 7.3: The PL spectrum of DQW in the zero magnetic field, $T \sim 1.4$ K, excitation power $0.5I_0$. The new bands A and B are clearly visible for applied bias $U_{nn} = -0.5$ and -0.7 V. The black lines are just guides for eye.

many-particle complexes (such as negatively or positively charged excitons).

The position of band A changes only slightly with U_{nn}, see Fig. 7.2. Thus Zvára *et al.* conclude that the band A should be related to the direct exciton DX localized in one well coupled to a hole from 2DHG in the adjacent well (positive trion). The band B should be related to the direct exciton DX localized in one well but coupled to an electron from the 2DEG in the adjacent well (negative trion). For details see [23].

7.1.1 Excitation dependence of PL spectra

Using the neutral density filters we changed the illumination conditions during our experiments. We could reduce the excitation power to 50%, 20%, 10%, 5%, 2% and 1% of its original value. The measurements for all these intensities were done in zero magnetic field under various applied biases and temperatures. We selected one illustrative set of spectra, see Fig. 7.4. It shows the excitation dependence of PL from DQW in zero magnetic field under $U_{nn} = -1.2$ V, $T = 5$ K. We will describe it in following paragraphs.
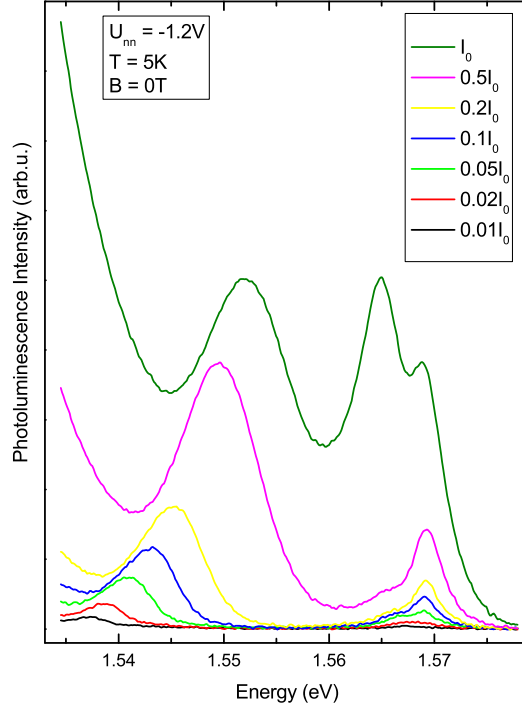
Figure 7.4: PL spectra of DQW as a function of the excitation power in the zero magnetic field, $T = 5$ K, $U_{nn} = -1.2$ V.

An immediately noticeable feature in Fig. 7.4 is the increasing of the PL intensity with the increasing excitation power, reflecting the apparent increase in the density of electron-hole pairs generated by this excitation. Let us note that with the rising excitation power the effective temperature of particles increases as well and therefore, lower excitation densities were preferred in our experiments. The majority of our experiments was done using 20% and 50% neutral density filters. We considered that as a reasonable compromise between the density of generated particles and the detected PL signal.

Another clearly recognizable feature seen in Fig. 7.4 is the shape of measured PL lines. For low excitation intensities only direct and indirect transitions are observed. A slight indication of another transition below the DX peak can be seen in the spectrum with 50% neutral density filter used (pink line). When no neutral density filter was used (100% excitation) third peak in energy below DX is clearly distinguishable (dark green line). We assume that this is a bound complex of particles, especially the negative trion (the reason why we identified it as negative trion and not positive will be explained later on in this chapter). There are enough free particles to bound such a complex when such a high excitation intensity is used. Moreover, the energy difference between negative trion and DX peak is ~3 meV which also supports our assumption to assign this third peak as the trion. It is not much higher than the reported value ~1.8 meV for negative trions in single QWs, see [21].
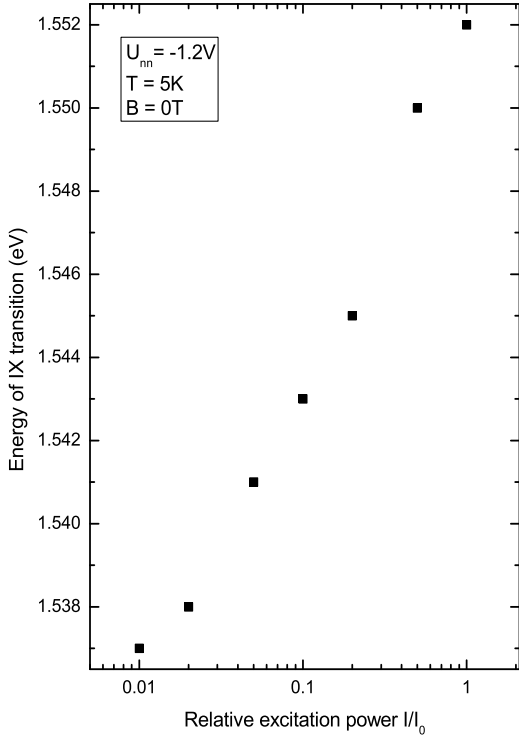
Figure 7.5: The IX energy as a function of the relative excitation power (in logarithmic scale) in the zero magnetic field at $T = 5$ K and under $U_{nn} = -1.2$ V.
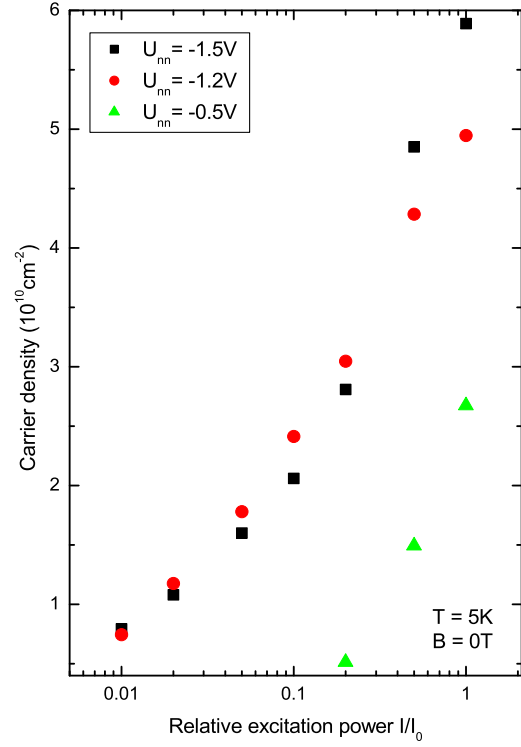
Figure 7.6: The dependence of the carrier density in DQW on relative excitation power (in logarithmic scale) for different values of U_{nn} in the zero magnetic field, $T = 5$ K.

Now we discuss the shift of the IX energy position with the excitation power. For the sake of clarity, this feature is depicted separately in Fig. 7.5. Please note that all excitation spectra are presented for $U_{nn} = -1.2$ V. Increasing the excitation power the energy of the IX transition increases as well. Concerning the energy of the IX transition, the increase of the excitation intensity at a constant U_{nn} is thus equivalent to the decrease of the applied bias on the structure at a constant excitation intensity. When many carriers are created they can screen the external electric field more efficiently. The tilt of DQW is then lower and the energy of IX transitions is willing to approach the energy of the direct ones, it increases.

It is noteworthy that the dependence of the IX energy on the excitation density can be roughly described by a logarithmic function, see Fig. 7.5. The similar study of the blueshift of the IX energy on the excitation power in biased coupled quantum wells was performed by Negoita et $al.$ [24]. Their sample consisted of a single pair of 6 nm-wide GaAs quantum wells separated by a 4.2 nm-wide $Al_{0.3}Ga_{0.7}As$ barrier, surrounded by thick, pure AlAs barriers. Negoita et $al.$ investigated the blueshift of IXs using a laser tuned to the DX resonance (therefore no free carriers were created). They observed similar behavior of the energy of the IX transition as a function of the excitation power as we did in Fig. 7.5. Their explanation of this logarithmic

increase supposes a linear shift at the low density which saturates to another linear shift at higher densities. In [24] Negoita *et al.* conclude that there are two ways how to envision a density-dependent IX blueshift. First free electrons and holes created by the laser screen out the perpendicular electric field or screen out the electron-hole Coulomb interactions. Second the energy shift is primarily a many-body effect of the exciton-exciton interactions. Negoita and co-workers proposed in [24] several different ways how to envision these interactions:

- the screening of the excitons by each other reduces the binding energy of the excitons,

- the excitons screen out the perpendicular electric field which reduces the quantum confined Stark shift,

- the long van der Waals attraction of the excitons is screened out, leaving a greater overall repulsion between the excitons due to Pauli exclusion,

- the excitons can be viewed as the repulsive point particles and the blueshift can be viewed as due to the mean-field interaction self-energy.

However, a proper theoretical treatment is still necessary. From time-resolved results Negoita *et al.* conclude that their blueshift of IX line (about 25 meV) is primarily a many-body effect caused by the large dipole-dipole interaction of the IXs, which is partially canceled by the effect of lattice heating at higher density (therefore they used two different linear shifts to describe it). They excluded the screening caused by free carriers due to the DX tuned laser.

We used the knowledge of the dependence of the IX peak energies on the excitation power to calculate approximately the density of photocreated carriers in our DQW. First the screened electric field $\tilde{\mathcal{E}}$ was calculated from the shift of IX transitions. The external electric field $\mathcal{E}$ is defined by applied bias voltage and the distance between the metallic contacts on the structure. Finally, we determined the density of carriers using the approximate concept that two wells of DQW can be assigned to two planes of the plane capacitor. Our computation is in accordance with the theory presented in [23] by Zvára *et al.*

$$\tilde{\mathcal{E}} = \mathcal{E} - \frac{\sigma}{2\varepsilon_0\varepsilon_r}, \tag{7.1}$$

where σ is the charge density in a single well (left of right) and $\varepsilon_r = 12.5$ is the relative dielectric constant. The calculated densities of photocreated carriers are depicted in Fig. 7.6. The results of our calculations refer to the comparable conditions of our sample to the Zvára's sample from the density point of view. We shell persist in their interpretation of A and B peaks here.
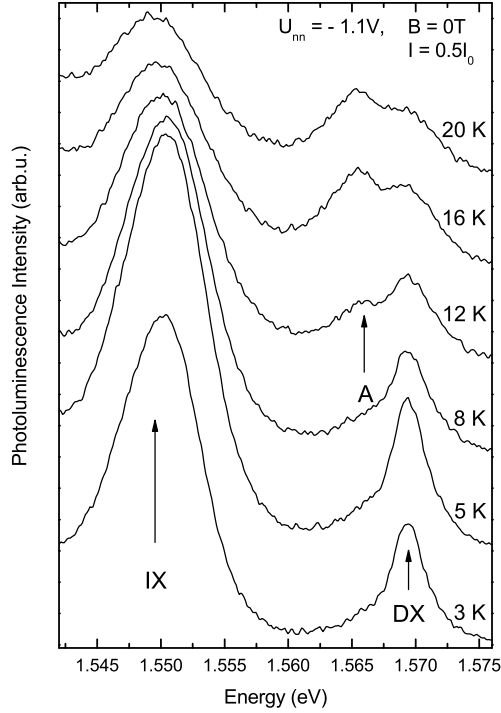
Figure 7.7: The temperature dependence of PL from DQW in the zero magnetic field under applied bias $U_{nn} = -1.1$ V, excitation power $0.5I_0$.

7.2 Measurements in in-plane magnetic field

Our measurements of PL from DQW in the in-plane magnetic field were motivated by the contradiction in experimental results published recently by our and other groups as was mentioned in Subsection 4.2.2. Since the recombination of IXs via localized states was proposed in recent papers [10, 11] of our group to overcome this contradiction we have decided to study the temperature dependence of IX PL to get some insight into the localization mechanism of IXs. We present here the measured spectra in zero as well as in finite in-plane magnetic fields and therefore a reasonable comparison can be made.

Let us focus the discussion on Fig. 7.7 with the temperature dependence of PL from DQW in the zero magnetic field at $U_{nn} = -1.1$ V for excitation density $I = 0.5I_0$. Increasing the temperature the PL of IX transitions remains clearly visible. Even at $T = 20$ K the IX transitions are well defined and distinguishable in the PL spectra. The relative decrease of the IX PL with increasing T is caused by thermally induced enhancement of the population of DX states. These states recombine much faster than the IX ones.

Another feature observable in Fig. 7.7 is a formation of new peak below the DX transitions which appears above $T = 12$ K. Its intensity increases simultaneously with the lowering of the DX PL. This peak corresponds to peak A in Fig. 7.3. It
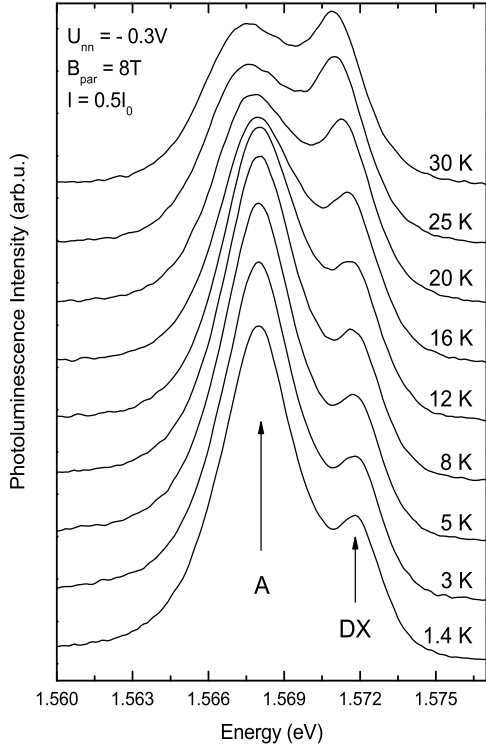
Figure 7.8: The temperature dependence of PL from DQW in the in-plane magnetic field 8 T at $U_{nn} = -0.3$ V for excitation power $0.5I_0$.
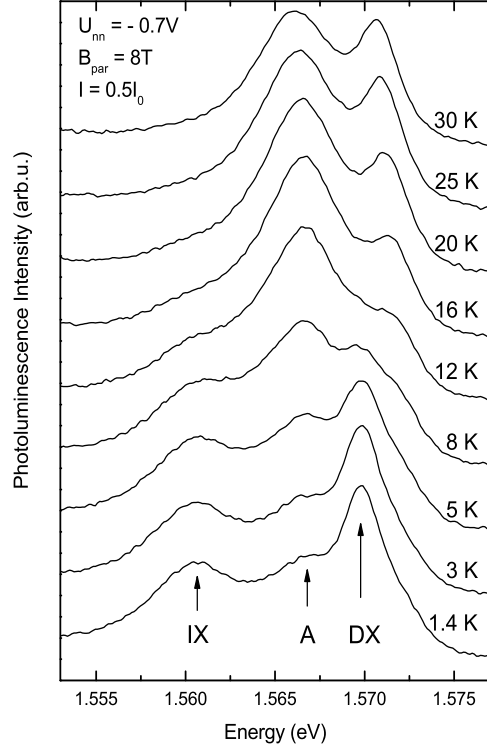
Figure 7.9: The temperature dependence of PL from DQW in the in-plane magnetic field 8 T at $U_{nn} = -0.7$ V for excitation power $0.5I_0$.

appears in all measured spectra in the in-plane magnetic field and will be discussed later on in this section.

Having discussed that the PL of IX transition does not vanish with increasing temperature in the zero magnetic field we present our measurements at the finite in-plane magnetic field of $B_\parallel = 8$ T. Two sets of PL spectra are shown. The first of them, Fig. 7.8, was taken at $U_{nn} = -0.3$ V where DX transitions and trions are observable, only. No IX transitions are present. The second set of measured spectra in Fig. 7.9 shows the PL of DQW under $U_{nn} = -0.7$ V. The DQW is already tilted enough and spatially indirect excitons are formed. We can surely identify the IX transitions within the temperature interval $\sim$1.4 K - 12 K. For T higher than 12 K the IX transitions are not recognizable in our spectra.

To explain this thermally induced quenching of IX PL line, we turn our attention to the basic theory presented in Subsection 4.2.1, which predicts the $B_\parallel$-induced damping of PL line arising from free indirect excitons. Let us assume that indirect excitons formed in our sample are not free but they are localized. In such a case there is a possibility for an indirect exciton to pass its momentum to the localization center and recombine in a radiative way. Consequently, the law of particle momentum conservation is fulfilled and the PL arising from these IX states can be observed.
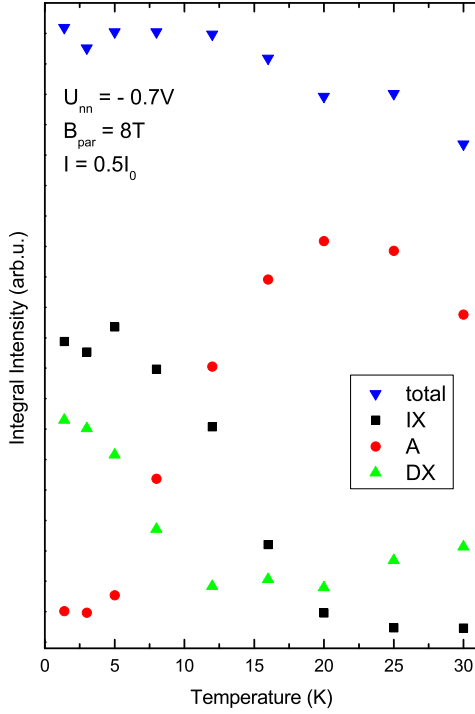
Figure 7.10: The temperature dependence of the integral intensity of PL from DQW in the in-plane magnetic field 8 T, $U_{nn} = -0.7$ V, excitation power $0.5I_0$.
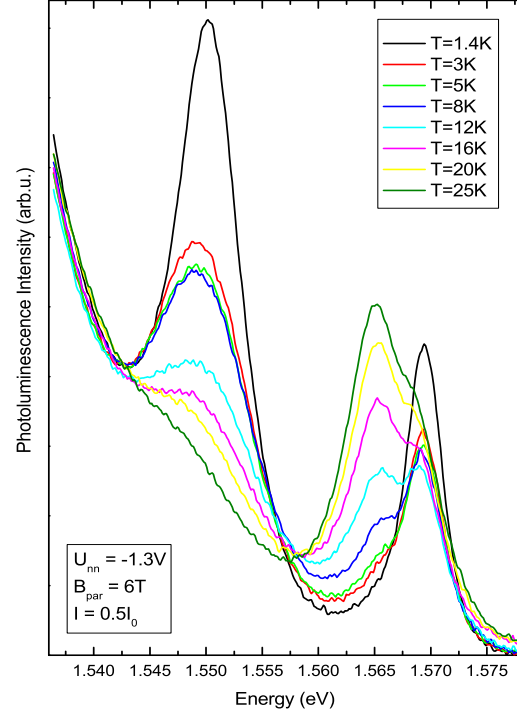
Figure 7.11: The temperature dependence of PL from DQW in the in-plane magnetic field 6 T under $U_{nn} = -1.3$ V, excitation power $0.5I_0$.

Increasing the temperature the localized indirect excitons become free due to the thermal excitation. They relax into the dispersion minimum which is placed at $\vec{P} = (|e|B_\parallel \Delta, 0, 0)$ in the reciprocal space. Hence, they are not optically active and consequently, the decline of IX PL is observed.

In our opinion, the above presented measurements elucidate the discrepancy among different works [8, 9, 10, 11] discussed in Subsection 4.2.2. Based on our findings we interpret the apparent contradiction as a result of different localization of IXs in different samples. The damping of IX concerns of free exciton PL, the steady IX PL corresponds to the PL of localized IX. The release of localized IX is caused by the temperature rise.

We will describe now the peak below the DX transition mentioned at the beginning of this section. The peak A is observable in the zero magnetic field as well as in the finite in-plane magnetic fields. We assume that this peak corresponds to the recombination of complex particle consisting of an electron or a hole bound to the neutral exciton, often referred to as the negatively or positively charged exciton. For low temperatures the intensities of IX and DX peaks are high and only a weak indication about formation of peak A is present. Increasing the temperature the intensity of IX peak decreases. The localized indirect excitons escape from locali-

zation centres and become free. Simultaneously, the intensities of DX and A peaks increase. We assume that free excitons bind another particle and form trions. This assumption is confirmed in Figs. 7.9 and 7.10 where the intensity of the peak A is higher than the intensity of the DX peak from $T = 8$ K up to $T = 25$ K. At $T = 25$ K the intensity of the peak A starts to decrease and simultaneously, the intensity of DX transition increases again. We assume that trions dissociate at this temperature into an exciton and another particle (an electron or a hole). If this interpretation is correct the intensity of DX peak should increase again. A weak indication of increasing DX intensity at T above 25 K is deducible in our spectra in Fig. 7.9 as well as in Fig. 7.10. Another hint that our assumptions about the rearrangement of particles from exciton into trionic states and vice versa are correct is given by the total integral PL intensity depicted in Fig. 7.10. While the intensities of individual peaks change with temperature the total integral intensity remains roughly the same. This finding confirms that none of recombination mechanisms is connected with a localization of recombining species on a particular defect, where one could expect a distinct increase of the nonradiative recombination. However, to proof our assumptions further measurements at higher temperatures should be performed.

We measured the temperature dependence of IX PL in the finite in-plane magnetic fields at various values of the magnetic field $B_{\parallel}$. We present here another set of PL spectra at $B_{\parallel} = 6$ T for an illustration in Fig. 7.11. In the left part of this figure the increasing intensity of all spectra is observed. It is the contribution from bulk GaAs as mentioned previously.

7.3   Measurements in perpendicular magnetic field

In this section, we present our measurements in the perpendicular magnetic fields up to $B_{\mathrm{per}} = 9$ T. We explain our assignment of peaks to the negatively and positively charged excitons as promised before. At first we will discuss the voltage dependence of PL from DQW attained at the excitation power $0.2I_0$. Our discussion will then continue with the excitation power dependence measured approximately at the same effective electric field on DQW.

Typical PL spectra of DQW in the perpendicular magnetic field as a function of applied bias U_{nn} are shown in Fig. 7.12. These particular spectra were taken at $B_{\mathrm{per}} = 9$ T, $T \sim 1.4$ K and the excitation power $I = 0.2I_0$. In experiment, we detected both circular polarizations of the emitted signal, i.e. the right-handed σ^+ and left-handed σ^- components. The assignment of the individual polarizations is in agreement with the theory presented by Vanhoucke *et al.* in [20]. It was confirmed as well from our experimental setup geometry. Red (blue) line stands for the σ^- (σ^+) polarization in all below presented PL spectra, respectively. Fig. 7.12 shows the behavior akin to Fig. 7.1 depicted for the zero magnetic field. The formation of direct and indirect transitions is nicely visible. The flat band regime was achieved
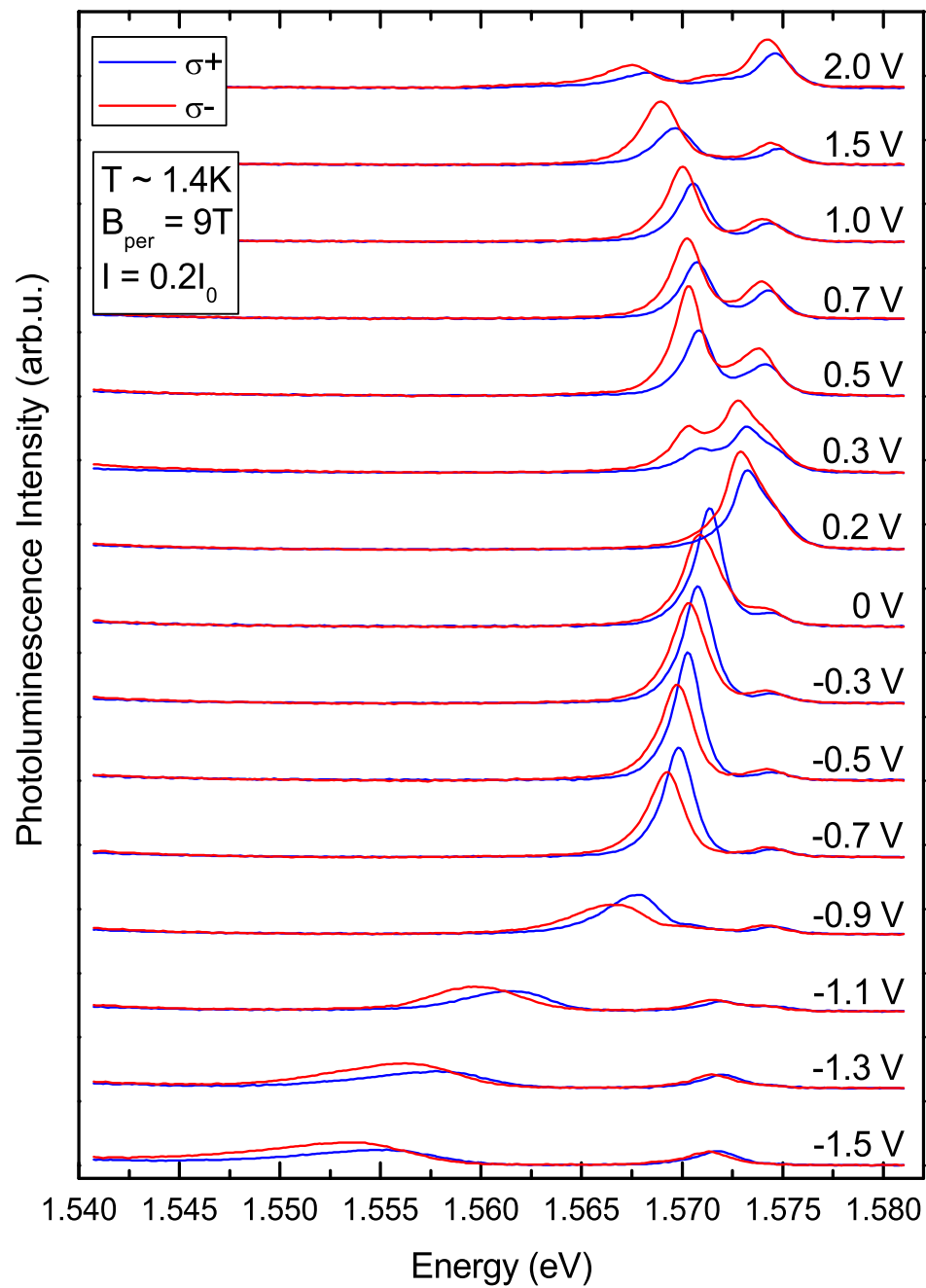
Figure 7.12: The PL of DQW for both polarizations σ^+ and σ^- in the perpendicular magnetic field 9 T at $T \sim 1.4$ K, excitation power $I = 0.2I_0$.
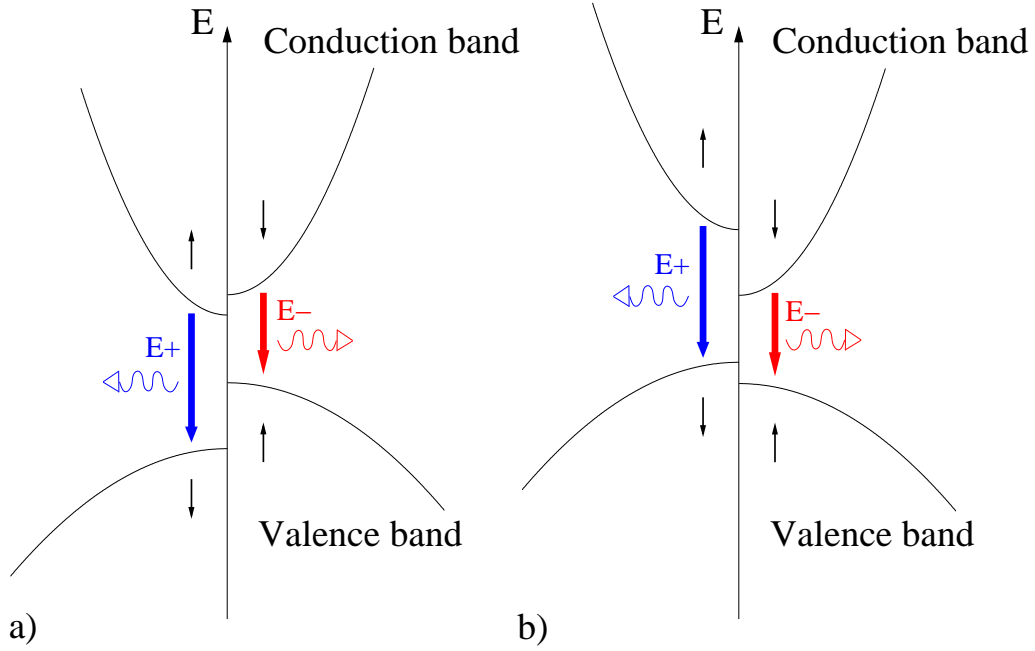
Figure 7.13: A schematic picture of two considered configurations of the valence and conduction bands according to the relation between g_e and g_h.

approximately at $U_{nn} \sim +0.2$ V.

One special feature of peaks below DX transition is worthy seeing in Fig. 7.12. Focusing our attention on spectra within the bias intervals $(-1.5$ V; -1.1 V$)$ and $(0.2$ V; 2.0 V$)$ we see that in energy lower lying transitions (σ^- polarization) show higher intensity than in energy higher lying ones. Taking account of the carrier thermalization, this behavior is expectable. Nevertheless, within the interval $(-0.9$ V; 0 V$)$ we see just the opposite.

We attempt to explain such a peculiarity using a simple model depicted in Fig. 7.13 where the conduction band for electrons and the valence band for heavy holes are sketched. Both bands are splitted into two parts, each half corresponds to one spin state of the particle (spin up ↑ or spin down ↓). Usually, the conditions $g_e < 0$; $g_h > 0$ and $|g_e| < |g_h|$ are supposed for g-factors in the system GaAs/AlGaAs. The model sketched in Fig. 7.13a is drawn in accordance with these assumptions. In the following discussion, we generally use symbols E^+ and E^- to denote upper and lower energies, respectively. We will even see that (for our data only and not in general) E^+ corresponds to the polarization σ^+ and E^- to σ^-.

The model in Fig. 7.13a describes well the observed intensity behavior of neutral excitons (EX). An electron e↑ with a hole h↓ recombine together on energy E^+ emitting a photon. An electron e↓ with a hole h↑ forming a neutral exciton recombine together on energy E^-. The splitting of the valence band plays a dominant role in this model. Due to the thermal occupation there are more holes with spin up h↑ and

therefore, the recombination process on energy E^- should be more pronounced in PL spectra. Our measurements confirm this conclusion. Unfortunately, this model fails when it is applied on the intensity behavior of charged excitons which are observed in Fig. 7.12.

We assign the peaks below DX transitions to the trions, in particular to the positive and negative trions for the positive and negative bias U_{nn}, respectively. We suppose that this fact results from the previously mentioned strong inhomogeneity in generation of electron-hole pairs above and under DQW. Applying positive U_{nn} holes are predominantly supplied into the well whereas the negative bias leads to the excess of electrons in the DQW. Henceforward, the positive and negative trions will be denoted as PT and NT, respectively.

Let us now discuss the positive applied bias and consequently the behavior of positive trions. In a very naive picture, two kinds of positive trions can be formed. They differ just in orientation of the electron spin as spin configuration of holes is given by the Pauli's exclusion principle. We will denote them as PT+ (e↑ h↓ h↑) and PT- (e↓ h↑ h↓).

(e↑ and h↓) recombine together from PT+ emitting a photon of energy E^+, leaving a hole h↑ in the valence band. In similar way, (e↓ and h↑) recombine together from PT- on energy E^- and a hole h↓ is left. We assume that there are more electrons with spin up e↑ due to the thermal distribution. As depicted in Fig. 7.13a E^+ is higher than E^- due to the bigger Zeeman splitting of the valence band. The transition at energy E^+ should be more pronounced in PL spectra as there are more electrons e↑. Its intensity should be higher than the intensity arising from PT- recombination on energy E^-. However, having a look at our data in Fig. 7.12 we realize that our results do not agree with this simple model. We observe exactly the opposite. Nevertheless, this discrepancy would be explained leaving assumptions $g_e < 0$; $g_h > 0$ and $|g_e| < |g_h|$ done previously.

Therefore, let us change these inequalities into the exactly opposite: $g_e > 0$; $g_h < 0$ and $|g_e| > |g_h|$. This will change the spin splitting of both bands resulting in the situation sketched in Fig. 7.13b. The splitting of the conduction band is now higher than the splitting for the valence band. We will discuss the negative trion, for completeness. Again, we get two possibilities how to form NT due to the Pauli's exclusion principle: NT+ (e↑ h↓ e↓) or NT- (e↓ h↑ e↑). In this case the splitting of the conduction band decides about the recombination energy. According to the scheme in Fig. 7.13b, the recombination energy E^+ is higher than E^-. We assume that there are more holes with spin down h↓ due to the thermal occupation. Thus the intensity of the NT+ recombination should be higher than the intensity arising from the NT- recombination. We really observe this behavior. In Fig. 7.12 we see that the higher energy peak shows higher intensity than the peak at the lower energy for negatively charged excitons within the bias interval $(-0.9 \text{ V}; 0 \text{ V})$.

Hence, our experimental data are in agreement with the suggested model just when in the system GaAs/AlGaAs unusual conditions $g_e > 0$; $g_h < 0$ and $|g_e| > |g_h|$ are taken into account. We are aware that this conclusion is rather ambitious, since

Table 7.1: The values of the effective g-factors of neutral excitons at various bias U_{nn} and magnetic field B_{per}. For empty spaces no corresponding spectrum was measured.

	9 T	8 T	7 T	6 T	5 T	4 T	2 T
2.0 V	0.68	0.67	0.39				
1.5 V	0.67	0.65	0.40	0.44	0.21	0.27	0.19
1.0 V	0.60						
0.7 V	0.62	0.64	0.42	0.43	0.19	0.11	0.16
0.4 V	0.63						
0.2 V	0.67	0.56	0.38	0.42	0.20	0.11	0
0 V	0.62	0.55	0.42	0.42	0.22	0.14	0
-0.5 V	0.63	0.65	0.48	0.43	0.27	0.15	0.06
-0.7 V	0.61						
-0.9 V	0.61						
-0.95 V	0.63						
-1.0 V	0.69	0.70	0.52	0.42	0.14	0.16	0.10

it contradicts the majority of up to now published experimental results. Another plausible explanation of the analyzed task is an improperly described source of the charging of DQW. We have expected above that the charge is supplied into DQW from the top contact, where most of the light is absorbed. This expectation, however, would not have been correct. At first, the absorption constant profile in the structure is not known well enough to describe absorption on both sides of DQW precisely. At second, the nonradiative recombination in the cap layer could be significantly higher than that in the substrate layer. Such effect would consequently revert above expected model conditions and the model 7.13a would be valid. Therefore, further experimental investigations in this direction are definitely necessary, as well as considerations about the relevance of the used theoretical model.

7.3.1 Effective g-factors

The PL signal from the studied sample has been investigated in a wider range of parameters than shown in Fig. 7.12. Different values of the perpendicular magnetic field were set up, as well as various values of the bias voltages were applied to the structure. We do not show all these spectra here as they exhibit very similar behavior as those in Fig. 7.12. We present the calculated values of the effective g-factors for neutral, indirect, positively and negatively charged excitons.

The g values were calculated in accordance with the theory presented in Chapter 5 by means of Eq. (5.26) where the quantity ΔE was taken as the Zeeman splitting between the circular polarizations σ^+ and σ^-. We found out that the g-factors for all bound complexes (EX, NT, PT) depend on the magnetic field. Moreover, there
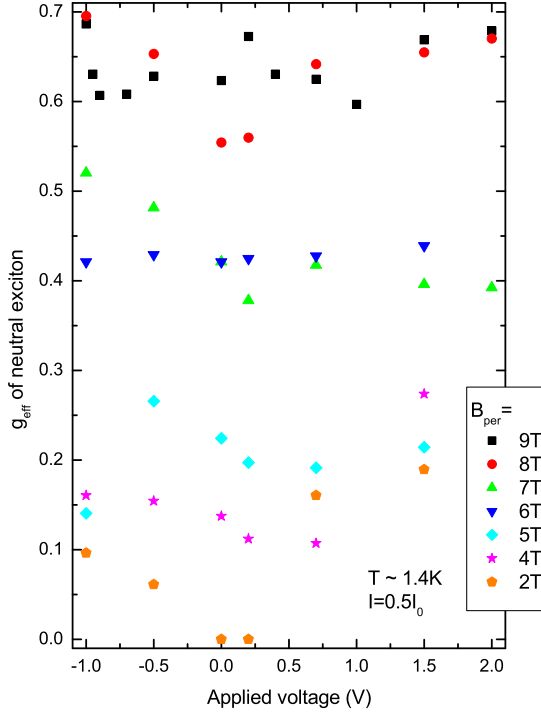
Figure 7.14: The voltage dependence of the effective g-factor of neutral exciton for various magnetic fields at $T \sim 1.4$ K, excitation power $I = 0.5I_0$.
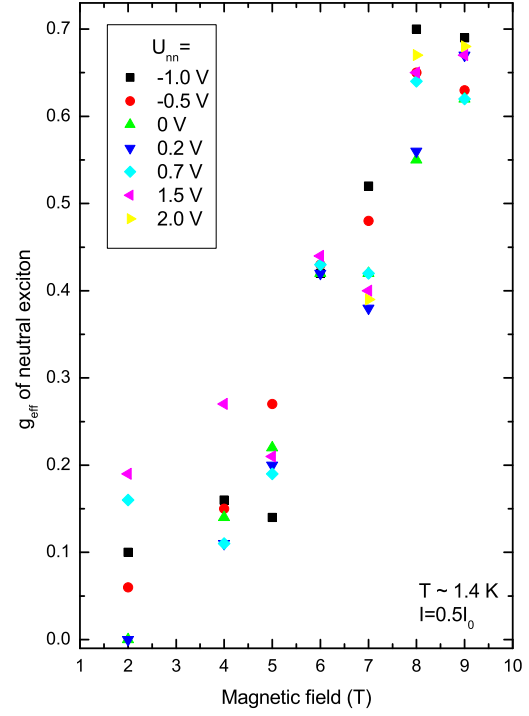
Figure 7.15: The magnetic field dependence of the effective g-factor of neutral exciton for various U_{nn} at $T \sim 1.4$ K, excitation power $I = 0.5I_0$.

is a rather strong dependence on the applied bias, especially for indirect excitons.

At first let us present our results for neutral direct excitons. All extracted values of the g-factor are summed up in Tab. 7.1 and depicted in Figs. 7.14 and 7.15. For low magnetic fields there is quite a big experimental error in determining the Zeeman splitting and thus the calculated g values have to be weighted with respect to this error. Based on our data, we conclude that absolute value of the g-factor tends to decline significantly with decreasing magnetic field for all measured U_{nn}.

Values summarized in Tab. 7.2 show that g_{eff} of IXs achieves at low magnetic fields considerably higher values than for neutral DXs. We assume that an electron and a hole forming IX are widely separated from each other in comparison to DXs. Therefore, their particular g-factors do not affect each other so much and finally do not give the zero limit for the effective g-factor of indirect exciton. Moreover, IX interact with the electron gas in the wells and their g-factor can be increased in this way. The calculated values of IX effective g-factor are 1.33, 1.44 and 2.12 for $U_{nn} = -1.0$ V, -1.3 V and -1.5 V at low magnetic fields, respectively.

Increasing the magnetic field the neutral exciton effective g-factor increases as well and reaches the value of 0.6 - 0.7 at $B_{per} = 9$ T. In these fields the surroundings of an exciton become polarized. The interaction of an exciton with surrounding, in
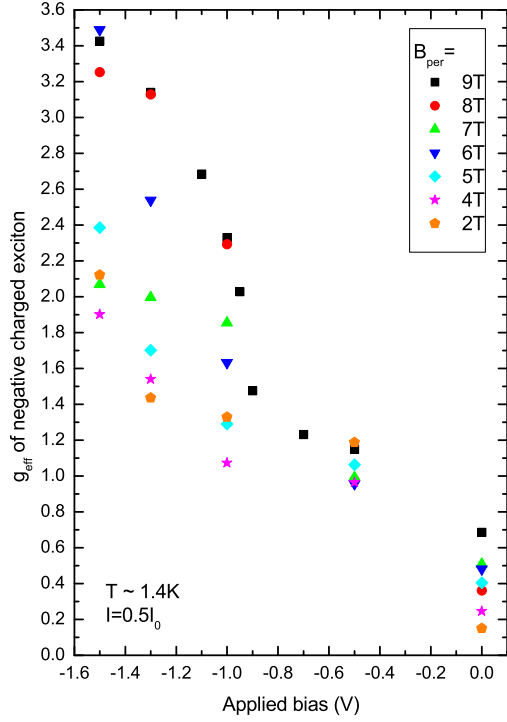
Figure 7.16: The voltage dependence of the effective g-factor of negatively charged and indirect exciton for various magnetic field at $T \sim 1.4$ K, excitation power $I = 0.5I_0$.
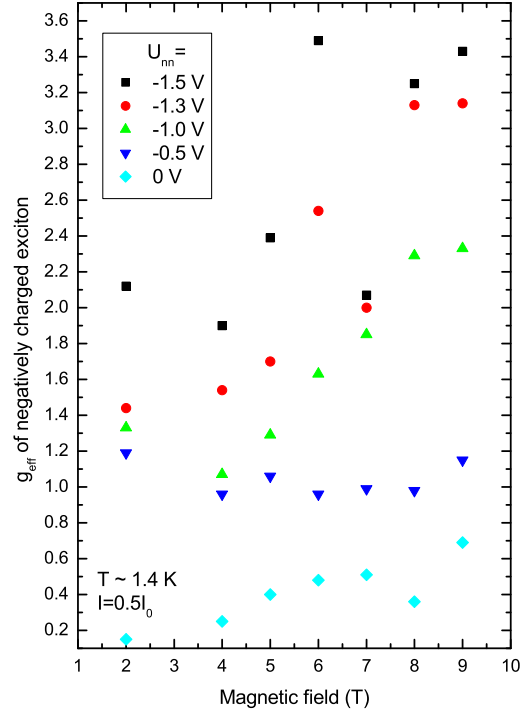
Figure 7.17: The magnetic field dependence of the effective g-factor of negatively charged and indirect exciton for various U_{nn} at $T \sim 1.4$ K, excitation power $I = 0.5I_0$.

spin polarized particles is of an order B_{per}^2 and has not been considered in Eq. (5.23). Hence, the g values can be increased at higher magnetic fields. The magnetic field dependence of the effective g-factor of the neutral exciton is shown in Fig. 7.15.

Now we compare our results with those already discussed in Section 5.3. Snelling *et al.* [15] showed that the sign of g-factor changes with the well width. They concluded that for narrow wells the sign of g-factor for the neutral exciton is negative. It should cross zero above $L \approx 7$ nm and further on remain positive. The well widths in our DQW are $\sim$8 nm. As can be seen from Tab. 7.1 all values of the effective g-factor are positive in accordance with Snelling's conclusions. Nevertheless, the comparison of results achieved on single and double QWs can be misleading.

Such an agreement is not attained when the result from Glasberg *et al.* [21] are considered. According to them, the g-factor of the neutral exciton is $\sim$0.5 for low magnetic fields then changes its sign and reaches the value of $\sim$-0.7 at fields above $B_{per} = 7$ T. The g values calculated from our measurements do not exhibit any sign reversal.

Another reference for g-factor of the neutral exciton can be found in Vanhoucke *et al.* [20]. The magnetic field dependence was investigated up to fields of 50 T. The reported g-factor of the neutral exciton was $\sim$1.5. We did not get such a high value

Table 7.2: The values of the effective g-factors of indirect excitons and negatively charged excitons for various bias voltage and magnetic field. The indirect exciton interacting with the electron gas in the wells appears from $U_{nn} \approx -0.9$ V down to $U_{nn} = -1.5$ V. For empty spaces no corresponding spectrum was measured.

	9 T	8 T	7 T	6 T	5 T	4 T	2 T
0 V	0.69	0.36	0.51	0.48	0.40	0.25	0.15
-0.5 V	1.15	0.98	0.99	0.96	1.06	0.96	1.19
-0.7 V	1.23						
-0.9 V	1.48						
-0.95 V	2.03						
-1.0 V	2.33	2.29	1.85	1.63	1.29	1.07	1.33
-1.1 V	2.68						
-1.3 V	3.14	3.13	2.00	2.54	1.70	1.54	1.44
-1.5 V	3.43	3.25	2.07	3.49	2.39	1.90	2.12

Table 7.3: The values of the effective g-factors of positively charged excitons for various bias voltage and magnetic field. For empty spaces no corresponding spectrum was measured.

	9 T	8 T	7 T	6 T	5 T	4 T	2 T
2.0 V	1.42	1.33	1.19				
1.5 V	1.32	1.14	0.96	0.66	0.68	0.42	0.47
1.0 V	1.08						
0.7 V	1.04	0.92	0.82	0.61	0.63	0.39	0.41
0.5 V	1.05						
0.4 V	1.04						

from our calculations, however, we worked with magnetic fields up to 9 T only. Nevertheless, there is an indication in Tab. 7.1 that the g value could rise with increasing magnetic field.

Let us focus our attention on the charged excitons now. The calculated g values of the negative trion and indirect excitons are summed up in Tab. 7.2 and depicted in Figs. 7.16 and 7.17. Similarly, the g values of the positive trion are presented in Tab. 7.3 and depicted in Figs. 7.18 and 7.19. The g-factors are remarkably higher than those for neutral exciton. We assume that it is caused by the presence of the third particle which effectively increases the g-factor of charged excitons. The change of their effective g-factors with the magnetic field is lower than it was for neutral excitons.

Now we discuss our accordance or contradiction with already published experimental data of other groups. A detailed summary of it was already provided in the Section 5.4. Glasberg *et al.* [21] reported positive signs of g-factors for low magnetic
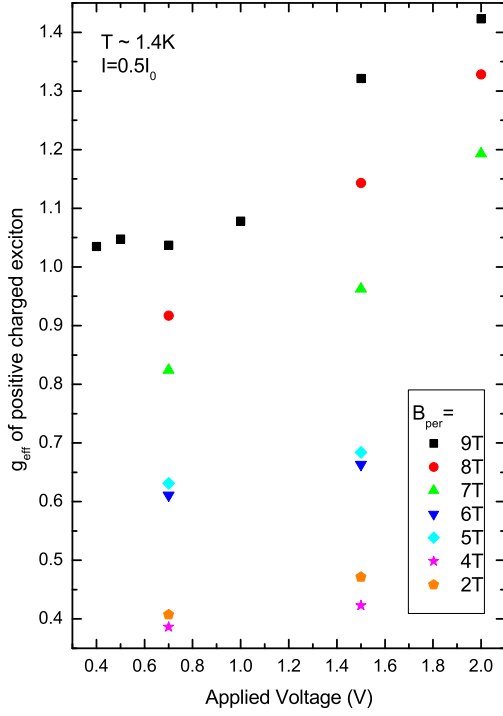
Figure 7.18: The voltage dependence of the effective g-factor of positively charged exciton for various magnetic fields at $T \sim 1.4$ K and excitation power $I = 0.5I_0$.
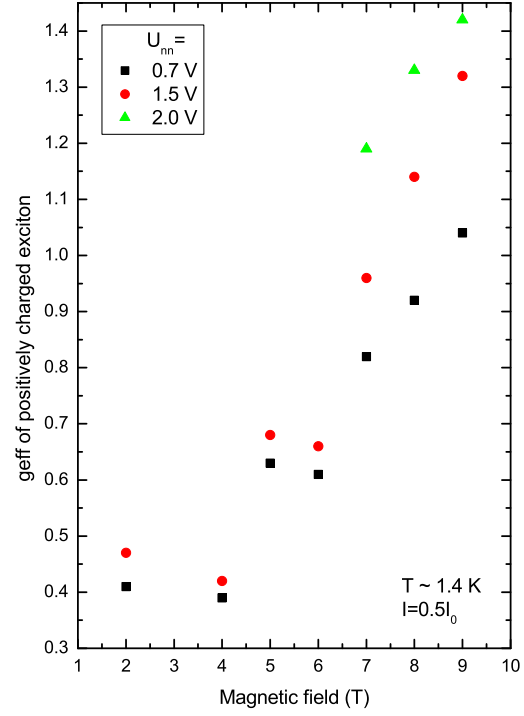
Figure 7.19: The magnetic field dependence of the effective g-factor of positively charged exciton for various U_{nn} at $T \sim 1.4$ K and excitation power $I = 0.5I_0$.

fields and estimated value of $\sim$0.5. Our measurements confirm the positive sign of g-factors for both types of charged excitons, but the absolute value of the g-factor only for the positive ones. Our calculated value of g-factor for negative trion is within the interval 0.15 - 1.33 and depends strongly on the applied bias voltage. Glasberg *et al.* observed the sign reversal and negative values of g-factors for fields above $B_{per} = 7$ T. Again, we are in contradiction with their measurements as we do not observe any sign reversal for charged excitons.

Let us recall the value of $\sim$1.9 for the g-factor of the negative trion in a single QW 10 nm-wide reported by Vanhoucke *et al.* [20]. The width of the investigated well is the closest value to our well widths $\sim$8 nm. Nevertheless, a direct comparison of Vanhoucke's results with our data is not possible as g-factor strongly depends on well width according to Snelling *at al.* [15]. However, we see that our values lying within the interval 0.15 - 2.33 are of the same order as those of Vanhoucke *et al.*. For the sake of completeness, we should mention that we are in contradiction to this work in one part, particularly in the magnetic field dependence of the g-factor of negatively charged excitons. Vanhoucke *et al.* did not observe any dependence on the magnetic field, but we do, see Tab. 7.2 and Fig. 7.17.

At the end of this subsection we summarize few basic outcomes of calculated

g-factors of indirect, neutral and charged excitons:

- The absolute value of the effective g-factor for a neutral direct exciton is in the limit of low magnetic fields significantly lower than for trions and indirect exciton.

- We observe a very strong dependence of g_{eff} on applied U_{nn}, especially for indirect excitons.

- We observe the magnetic field dependence of g_{eff} for all bound complexes.

- We do not observe any sign reversal of g_{eff} for all bound complexes.

7.3.2 Excitation dependence of PL spectra

Having investigated the g-factors of trionic and excitonic states in DQW, an appealing question about the origin of a strong rise of the g-factor for IXs appeared. This dependence is clearly seen in Tab. 7.2 or in Fig. 7.16. In order to find an explanation for it, we have established two basic models and performed the experiment to find out some arguments allowing of the decision about their relevance. At first we describe these models and after that we show achieved experimental data.

The first model supposes an increase of IX g-factor due to the interaction with other particles in the DQW. Since the tilting of DQW leads to the increase of the IX lifetime and consequently to the rise of their density, the enhanced g-factor of IXs would simply reflect the increased strength of the many-body interactions at higher IX concentrations.

The second model is related to the barriers surrounding both wells. Since the g-factors of electrons and holes in the quantum well and in the barriers strongly differ, cf. e.g. g-factors for the electron $g_e = -0.44$ in bulk GaAs and $g_e = 0.42$ in bulk $Al_{0.33}Ga_{0.67}As$ [2], any changes in probabilities of particles to be found in barriers should strongly affect the observed g-factor. As the tilting of DQW induced by the applied bias U_{nn} strongly modifies electron and hole wavefunctions, the experimentally observed increase of g-factor could be given by the change of the tunneling efficiency into surrounding barriers.

The PL from DQW was measured in the perpendicular magnetic field $B_{per} = 9$ T under various excitation intensities. The temperature was set to ~ 1.4 K. A particular bias U_{nn} was chosen for each excitation power in order to achieve approximately the same tilting of the DQW. In other words, the energy of the IX transition was kept constant. The measured spectra are presented in Fig. 7.20. The values of excitation power and applied bias are written nearby each corresponding PL line.

The Zeeman splitting and the ratio of peak intensities σ^+/σ^- were extracted from PL spectra in Fig. 7.20 and plotted into Fig. 7.21. We did not find any noticeable effect that the Zeeman splitting changes within the interval of used excitation
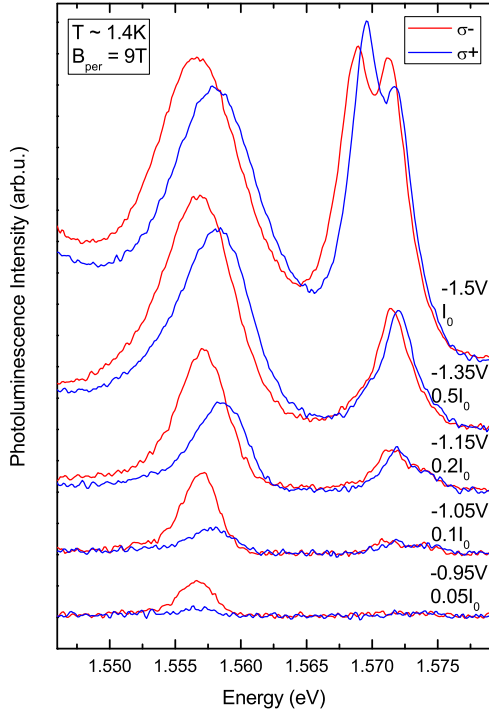
Figure 7.20: The excitation dependence of PL intensity for both polarizations σ^+ and σ^- in the perpendicular magnetic field 9 T at $T \sim 1.4$ K measured approximately at the same effective electric field inside the structure.
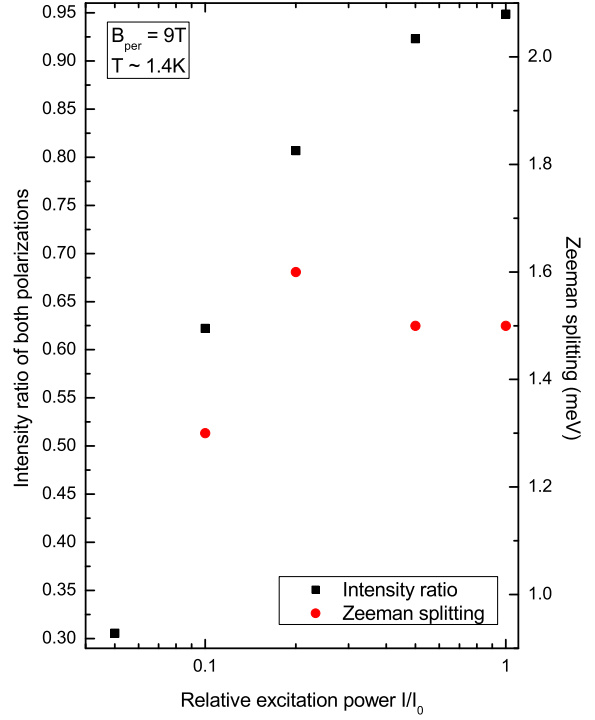
Figure 7.21: The dependence of the Zeeman splitting and intensity ratio (counted for IX peaks) of both polarizations σ^+ and σ^- on the excitation power (in logarithmic scale).

powers. It remains almost the same within the experimental error for all excitation power used[1] but the intensity ratio dramatically changes with the change of excitation power.

No noticeable change of Zeeman splitting indicates that the effective g-factor of indirect excitons remains unaffected by the IX density inside DQW, which contradicts the first suggested model. Therefore, the second proposed model seems to be more appropriate. Unfortunately, the lack of published experimental data does not allow a comparison of these results with independent ones.

Nevertheless, even though the second model seems to be more suitable, the first one cannot be simply refused. The decrease of the excitation density, causing the damping of the IX concentration, simultaneously leads to the strong decline of the effective temperature of the IX gas. This lowered temperature brings about stronger spin polarization as clearly seen from the ratio σ^+/σ^- depicted in the Fig. 7.21. This enhanced polarization strengthens the many-body interactions in the IX gas and can at least partially compensate the effects of decreasing IX density.

_____

[1] It was not possible to extract the Zeeman splitting value for excitation power $0.05I_0$. The position of IX peak for σ^+ polarization is not well defined.

Since the achieved data do not allow a definite decision on the relevance of both models further experiments are desirable. In particular, measurements in a wider range of excitation densities would certainly help in the explanation of the discussed effect and should be therefore realized.

Chapter 8

Conclusions

We summarize the main achieved results of this diploma thesis in the next paragraphs.

- The PL spectra of DQW were measured in dependence on electric and magnetic fields, different excitation power as well as on various temperatures. Due to our experimental setup and geometry of the sample we could observe simultaneously both the neutral and charged excitons within the same sample.

- The special attention was given to the temperature dependencies of the indirect transitions in the finite in-plane magnetic field. For low temperatures no damping of IX PL was observed. To explain the discrepancy between our group (no IX PL damping) and Parlangeli's group (the IX PL damping was observed at low fields) a simple model of localized indirect excitons was discussed. Our measurements partly confirm the model of IX localization which was proposed by our group few years ago. In this thesis presented experimental results really indicate that the localization of IX plays a crucial role in IX recombination.

- The Zeeman splitting was determined from many polarization-distinguished spectra for various values of U_{nn} and perpendicular magnetic field. Thereafter the effective values of g-factors were calculated for the direct and indirect, as well as neutral and charged excitons. We proposed and discussed few models to describe the behavior of g_{eff}. We found out that the g values are rather small for neutral exciton at low fields (almost equal to zero) while they are approaching much higher values for charged and indirect excitons. Only few publications can be found on this topic and some of them are in the contradiction with each other. Therefore, further experiments need to be performed so some definite conclusions can be formed on the basis of observed data.

Bibliography

[1] G. Bastard: *Wave mechanics applied to semiconductor heterostructures.* Monographies de physique, Paris, (1992).

[2] J.H. Davies: *The Physics Of Low-dimensional Semiconductors, An Introduction.* Cambridge University Press, Glasgow, (1998).

[3] M. Orlita: *Studium kvantových jam v systému GaAs/GaAlAs - diploma thesis.* MFF UK, Prague, (2002), in Czech.

[4] S.K. Lyo: *Transport and level anticrossing in strongly coupled double quantum wells with in-plane magnetic fields.* Phys. Rev. B 50, 4965, (1994).

[5] A.A. Gorbatsevich and I.V. Tokatly: *Formation of k-space indirect magnetoexcitons in double-quantum-well direct-gap heterostructures.* Semicond. Sci. Technol. 13, 288, (1998).

[6] K. Chang and F.M. Peeters: *Bright-to-dark exciton transition in symmetric coupled quantum wells induced by an in-plane magnetic field.* Phys. Rev. B 63, 153307, (2001).

[7] A.Parlangeli, P.C.M. Christianen, J.C. Maan, I.V. Tokatly, C.B. Soerensen and P.E. Lindelof: *Optical observation of the energy-momentum dispersion of spatially indirect excitons.* Phys. Rev. B 62, 15 323, (2000).

[8] A. Parlangeli, P.C.M. Christianen, J.C. Maan, C.B. Soerensen and P.E. Lindelof: *Spatially indirect excitons in $GaAs/Al_{0.35}Ga_{0.65}As$ double quantum wells in the presence of in-plane magnetic fields.* Phys. stat. sol. (a) 178, 45, (2000).

[9] L.V. Butov, A.V. Mintsev, Yu.E. Lozovik, K.L. Campman and A.C. Gossard: *From spatially indirect excitons to momentum-space indirect excitons by an in-plane magnetic field.* Phys. Rev. B 62, 1548, (2000).

[10] M. Orlita, R. Grill, M. Zvára, G.H.Döhler, S. Malzer, M. Byszewski and J. Soubusta: *Luminescence of coupled quantum wells: Effects of indirect excitons in high in-plane magnetic fields.* Phys. Rev. B 70, 075309, (2004).

[11] M. Orlita, R. Grill, M. Zvára, G.H.Döhler, S. Malzer, M. Byszewski and J. Soubusta: *Luminescence of indirect excitons in high in-plane magnetic fields.* Physica E 30, 1, (2005).

[12] A.S. Davydov: *Kvantová mechanika.* SPN, Prague, (1978), in Czech.

[13] J. Formánek: *Úvod do kvantové teorie II.* Academia, Prague, (2004), in Czech.

[14] H.W. van Kesteren, E.C. Cosman, W.A.J.A. van der Poel, C.T. Foxon: *Fine structure of excitons in type II GaAs/AlAs quantum wells.* Phys. Rev. B 41, 5283, (1990).

[15] M.J. Snelling, E. Blackwood, C.J. McDonagh, R.T. Harley, C.T.B. Foxon: *Exciton, heavy-hole, and electron g factors in type I $GaAs/Al_xGa_{1-x}As$ quantum wells.* Phys. Rev. B 45, 3922, (1992).

[16] M.J. Snelling, G.P. Flinn, A.S. Plaut, R.T. Harley, A.C. Tropper, R. Eccleston, C.C. Phillips: *Magnetic g factor of electrons in $GaAs/Al_xGa_{1-x}As$ quantum wells.* Phys. Rev. B 44, 11 345, (1991).

[17] A.J. Shields, M. Pepper, M.Y. Simmons, and D.A. Ritchie: *Evolution of GaAs quantum well excitons with excess electron density and magnetic field.* Solid-State Electronics 40, 275, (1996).

[18] E. Tutuc, S. Melinte, and M. Shayegan: *Spin polarization and g factor of a dilute GaAs two-dimensional electron system.* Phys. Rev. Letters 88, 036805, (2002).

[19] Y.Y. Proskuryakov, A.K. Savchenko, S.S. Safonov, M. Pepper, M.Y. Simmons, and D.A. Ritchie: *Hole-hole interaction effect in the conductance of the two-dimensional hole gas in the ballistic regime.* Phys. Rev. Letters 89, 076406, (2002).

[20] T. Vanhoucke, M. Hayne, M. Henini, V.V. Moshchalkov: *Magnetophotoluminescence of negatively charged excitons in narrow quantum wells.* Phys. Rev. B 63, 125331, (2001).

[21] S. Glasberg, G. Finkelstein, H. Shtrikman, and I. Bar-Joseph: *Comparative study of the negatively and positively charged excitons in GaAs quantum wells.* Phys. Rev. B 59, R10 425, (1999).

[22] F.J. Teran, L. Eaves, L. Mansouri, H. Buhmann, D.K. Maude, M. Potemski, M. Henini, and G. Hill: *Trion formation in narrow GaAs quantum well structures.* Phys. Rev. B 71, 161309, (2005).

[23] M. Zvára, R. Grill, P. Hlídek, M. Orlita and J. Soubusta: *Photoluminescence of biased $GaAs/Al_xGa_{1-x}As$ double quantum wells - many-body effects.* Physica E 12, 335, (2002).

[24] V. Negoita, D.W. Snoke and K. Eberl: *Huge density-dependent blueshift of indirect excitons in biased coupled quantum wells.* Phys. Rev. B 61, 2779, (2000).